# Fibre Reinforcement Effects in Tuning EV Release of Hydrogels

Anne Zijl
Student no. : 2817233
a.zijl@students.uu.nl
Dept. Orthopaedics
RMCU

# Fibre Reinforcements in Tuning EV Release of Silk Hydrogels


## Abstract:

The heart has a limited capacity for regeneration following trauma due in part to a low presence of cardiac stem cells. Previous literature has shown that cardiac regeneration may be boosted in the short term by promoting angiogenesis through the addition of certain growth factors present in cardiac stem cells as well as those in endothelial derived extracellular vesicles. To support cardiac angiogenesis more effectively, we propose that an extended-release window of these factors is necessary. The aim of this study is to create a cell-free extracellular vesicle-laden hydrogel system that releases extracellular vesicles over such an extended period (14 days). We went with a casted product; however, 3D extrusion printing may be considered in future research to increase control and resolution of the product, the product being a cardiac patch containing extracellular-vesicle-loaded hydrogels. For this hydrogel system, both gelatine methacryloyl and silk fibroin-based hydrogels were investigated, using lithium phenyl-2,4,6-trimethylbenzoylphosphinate and a combination of riboflavin and sodium persulfate as photocrosslinkers, respectively. The former was used in combination with ultraviolet light, whereas the latter initiated photocrosslinking through visible light. The degradation kinetics, mechanical properties, permeability, and extracellular vesicle release kinetics of our hydrogels were investigated and may be tuned through the varying gel precursor concentration and integration of a supporting melt electrowritten polycaprolactone mesh scaffold featuring a hexagonal structure.



**Keywords:** Acute myocardial infarction, extracellular vesicles, hydrogels, GelMA, silk fibroin


## Non-technical summary:

Due to the low turnover of stem cells in the heart, there is a need for solutions that help boost the organ's regenerative capacity. In this research, we propose the generation of a cardiac patch to fulfil that role. This patch would consist of a silk-based or gelatine methacryloyl-based hydrogel that is loaded with extracellular vesicles (a type of vesicle that buds off of cells and is filled with factors that promote and support tissue regeneration). As tissue regeneration takes a significant amount of time, we selected a release window of 14 days and analysed the release of extracellular vesicles over this time. 14 days was selected because this is on average how long it takes for blood vessels to form. Because hydrogels are generally quite weak and tend to release extracellular vesicles and other small particles quite quickly, we introduced within our gel a 3D printed biodegradable biocompatible polyester mesh with a hexagonal microstructure to provide reinforcement. Within our study, we compared two types of gel, one based on gelatine and the other on silk fibroin. Solutions with these precursors were both gelated using light (visible light in the case of the gelatine-based hydrogel and UV-light in the case of the silk-based hydrogel). This was made possible through the addition of a molecule which initiates the formation of crosslinks within the hydrogel when under the influence of the relevant light source. Results from our research suggest that silk-based hydrogels are able to delay extracellular vesicle release, more so than gelatine-based hydrogels. In addition, it is found that the dynamics of the environment the hydrogels reside in is an incredibly important factor with regards to controlling the extracellular vesicle release window.

# Index

# 1. Introduction and background information:

## 1.1 Purpose of the study

The purpose of this study is to analyse the differences in extracellular vesicle (EV) release properties from cell-free EV-laden casted hydrogel systems, either with or without added support from a melt electrowritten PCL mesh, depending on hydrogel selection, hydrogel precursor concentration, and the presence of a melt electrowritten mesh. These constructs are thought to be able to boost cardiac regeneration through promoting angiogenesis in the heart after a cardiac event resulting in major loss of cardiomyocytes. In the past, however, the effectiveness of such constructs releasing EVs has been limited due to a burst-release pattern. For the purposes of our study, we aim to find ways in which to prolong this release window to enhance the effectiveness of EVs in their promotion of angiogenesis. In order to investigate how this release window can be tuned, extracellular vesicle release studies were conducted on the aforementioned groups, where hydrogels were either gelatine methacryloyl (GelMA) or silk fibroin (SF) based and were crosslinked either with lithium phenyl-2,4,6-trimethylbenzoylphosphinate (LAP), or a combination of riboflavin and sodium persulfate, respectively. In order to expand on the results of these EV release tests, tests were done to assess the mechanical and degradation properties of the different gels, concentrations, and in the presence or absence of a mesh within the casted hydrogel sample. Our hypothesis and expectation was that hydrogel systems featuring silk fibroin would result in prolonged EV release windows due to reduced hydrogel degradation over time. In addition, higher concentrations of hydrogels, and hydrogels incorporating a MEW mesh are expected to feature shorter EV release windows due to an increase in stiffness and mechanical strength. Lastly, we hypothesise that dynamic loading, as is present in the dynamic environment of the heart, will quicken EV release. This last hypothesis was investigated through a dynamic loading EV release test.

## 1.2 Cardiovascular diseases

According to reports by the Central Bureau of Statistics (2021) in the Netherlands, cardiovascular diseases have long been one of the main causes of death, missing out on the top spot only in the last couple of years when that spot was claimed by cancer. In 2020 alone, the top three killers (cancer of all types, cardiovascular diseases, and COVID19) accounted for 47,046, 36,579, and 20,138 deaths respectively. Accounting for over a fifth of all deaths in the Netherlands in 2020 and acting as the leading cause of death worldwide (Ritchie & Roser, 2018). Clearly there is still much to be gained in the treatment of cardiovascular diseases.

Cardiovascular diseases such as acute myocardial infarction (AMI) result in a major loss of the number of functional cardiomyocytes, which are replaced by fibrous scar tissue (Vettori et al., 2020). The heart is maladapted to regenerate an adequate number of cardiomyocytes sufficient to re-establish full functionality and adequate cardiac output, with cardiomyocyte turnover rate estimations in adults ranging from 1% to 4% (Buikema et al., 2013). In addition, the number of cardiac stem cells (CSCs) is very low, and CSCs are therefore suggested to be capable of remodelling only occurrences of minor damage rather than catastrophic cardiomyocyte loss (Koudstaal et al., 2013). Indeed the number of stem cells in the heart is so low, that it had long been presumed that the heart contains no stem cells at all. This was thought to be so since AMIs consistently lead to fibrosis and eventual scar formation rather than regeneration of functional tissue. However, the discovery of cardiac stem cells has slowly begun to change the view of the heart as a post-mitotic organ (Fine & Vunjak-Novakovic, 2020).

It has been suggested that stem cells such as those derived from bone marrow or CSCs may excrete cytokines and growth factors that are beneficial in the differentiation and regeneration of cardiomyocytes, and that the application of additional CSCs in patients who have endured an AMI may therefore improve general cardiac health and reduce fibrosis. Early results from research using bone marrow-derived stem cells for the treatment of AMI were promising, as patients showed an initial increase of the left ventricular ejection fraction (LVEF; Assmus et al., 2002). Sadly, after a 5-

year follow up of the trial, it became clear that the effects were not to last, as no long-term beneficial effects were found (Meyer et al., 2006). Other studies using bone-marrow derived stem cells and a wide variety of stem and progenitor cells have found similarly modest long-term results, showing an initial improvement to the LVEF that drastically reduces to negligible amounts within months (Buikema et al., 2013). A major problem with the injection of CSCs and cardiac progenitor cells is that of poor cell retention and survival after application (Cambria et al., 2017). So far, injection with stem cells has been an insufficient measure in guaranteeing long-term proliferation and differentiation of cardiomyocytes towards the goal of cardiac regeneration. Therefore, other avenues must be pursued that support and ameliorate the longevity of these transplanted cells.

### 1.3 Extracellular vesicles

The initial beneficial effect of treatment with stem cells has been suggested to be because of the underlying paracrine effect of certain cytokines, chemokines, and growth factors. Several factors have been identified as playing key roles in angiogenesis, namely: vascular endothelial growth factor (VEGF), transforming growth factor-β (TGF-β), platelet-derived growth factor (PDGF), and fibroblast growth factor (FGF), where FGF and VEGF stimulate the proliferation of endothelial cells, which in turn stimulate the secretion of other pro-angiogenic growth factors (Vettori et al., 2020). These factors play a role in stimulating endothelial proliferation, and some have the additional effect of stimulating endothelial cell migration, which is crucial in the revascularization of fibrotic scar tissue in the heart after infarction.

Efforts have been made in coming up with more long-lasting ways of administering these factors without the need for stem cells, which can be difficult to harvest in sufficient amounts. One proposed solution is the use of extracellular vesicles (EVs). EVs are lipid-coated messenger particles released by most types of cells, including stem cells and all major cardiac cell types, and they can transport a wide variety of bioactive components (i.e., proteins, second messengers, mRNA, miRNA, lipids, parts of organelles, etc.(Rezaie et al., 2019; Sluijter et al., 2018). EVs consist of a phospholipid bilayer encapsulating the molecules to be transported. They are released from all cells between 20 and 1000 nm in size studied to date and they can be divided into several subtypes, namely: exosomes (with diameters ranging from ~30-150 nm), microvesicles (100-1000 nm), and apoptotic bodies (50-5000 nm and released from dying cells;  Hafiane & Daskalopoulou, 2018; ;Mol et al., 2019, Rezaie et al., 2019). EVs have been found to aid in tissue repair by inducing differentiation of stem cells, initiating angiogenesis by promoting matrix degradation (especially for EVs containing metalloproteinase proteins), and acting as a major pathway for several secretory proteins such as IL-1β (Gaceb et al., 2014). Three mechanisms are known by which EVs are taken up: internalization, direct fusion, and receptor-ligand interaction (Rezaie et al., 2019). Because of their important role in the regulation of angiogenesis and their capacity for storing and delivering paracrine factors, EVs, especially exosomes, have been a promising candidate for use in treatment of ischaemic heart disease, AMI, and heart failure (Li et al., 2021; Sluijter et al., 2018). In fact, the paracrine effect caused by mesenchymal stem cells is thought to be primarily attributable to EVs, although this may be dependent on EV origin, as protein content of EVs is largely dependent on the cell type from which the EV is derived (Doyle & Wang, 2019; Lee et al., 2012). In addition, EVs are considered good candidates for therapeutic drug delivery because of their non-toxic and biocompatible nature, providing EVs with the capacity for easy distribution throughout the body without being attacked and degraded by the immune system (Maheshwari et al., 2017). Previous research done by Arslan et al. (2013) showed that cardiac infarct size in mice could be reduced to 50% with a single injection of purified exosomes. Subsequent systemic inflammation could also be reduced by treatment with these exosomes (Arslan et al., 2013).  The usage of EVs has additional benefit over cell-based therapies in that it allows for greater product stability, biocompatibility, and dosage control, as well as enhanced suitability for (genetic) engineering (Rogers et al., 2020).

The composition of an EV is highly dependent on the cell from which it is derived, as EVs have many functions, and the paracrine factors they contain are a reflection of that function. In addition, it has been proposed that the protein content of the EVs is largely dependent on the extraction method

used (Doyle & Wang, 2019). Cells reported to release EVs with cardioprotective and pro-angiogenic roles include stem cells derived from adipose and human umbilical cord, as well as bone marrow-derived mesenchymal stem cells (Hromada et al., 2017). EVs derived from endothelial cells have been shown to promote angiogenesis at concentrations similar to those found *in vivo*, while at higher concentrations angiogenesis was inhibited (Hromada et al., 2017). This is likely due to an over-expression of pro-angiogenic paracrine factors (i.e., VEGF and HIF-1α) which increases risk of haemorrhage by disrupting tight junctions (Li et al., 2021). Another source of EVs with cardioprotective potential are from cardiomyocytes (CM) derived by differentiating human induced pluripotent stem cells (hiPSCs). Due to their superior ease of isolation, hiPSCs are of great interest for applications which suffer from the difficulty in isolating large amounts of stem cells. EVs derived from such cells have already been shown to be taken up by cardiac and endothelial cells and to have pro-angiogenic effects in human vascular endothelial cells (HUVEC) as well as promoting cell proliferation in cardiac committed cell populations (Louro et al., 2022). When comparing cell migration in promoting wound closure as an effect of EV treatment, hiPSC derived EVs were observed to have superior results when compared to results from EVs derived from other sources (Louro et al., 2022). For the purposes of this study, EVs were derived from hiPSCs differentiated to cardiomyocytes to make use of these superior pro-proliferative effects. However, endothelial EVs have been known to have a deleterious role in angiogenesis when present in higher concentrations and it is unclear if high concentrations of hiPSC-derived EVs would have the same effects. As such, EV release may have to be tightly controlled. The contents and surface structure of EVs may be modified to improve cardiac targeting and pro-angiogenic behaviour, this is however out of the scope of this research (Pezzana et al., 2021).

Much is still unknown about the biosynthesis of EVs, there exist no current standardized methods for isolation, purification, characterisation, and storage. Even so, great strides have been made in the past couple years, and bit by bit a greater understanding of EVs is emerging (Davidson et al., 2022; Hafiane & Daskalopoulou, 2018). For now, EV characterisation and identification remains difficult because of a lack of known markers that may be used to identify EV origin, as well as due to the challenges brought along by their small sizes (Davidson et al., 2022; Hromada et al., 2017). For example, at first tetraspanin proteins were thought to be biomarkers specific to exosomes, but these have recently been found to be exhibited by both microvesicles and apoptotic bodies (Doyle & Wang, 2019). Even so, a differentiation may be made in EV type (microvesicle, exosome, or apoptotic body) depending on EV protein content through mass spectrometry due to the differences in the formation of these different types of EVs (Doyle & Wang, 2019). In addition, much work has been done in recent years to identify miRNA expression by EVs of different origins (Louro et al., 2022). The most prevalent techniques used to identify and quantify EVs are resistive pulse sensing (RPS), and nanoparticle tracking analysis (NTA), both methods relying on light scattering. Although a differentiation between EV origins is difficult to make through investigation of marker proteins, marker proteins for EVs in general do exist and can be used to quantify EVs through ELISA or western blots (Davidson et al., 2022). In the case of, e.g., endothelial cell derived EVs, several surface markers are expressed through which the EV may be characterised, but none of these is expressed exclusively by these vesicles, making it necessary to investigate the presence of a combination of markers through flow cytometry (including but not limited to: CD31, CD54, CD62E, CD105, CD144, CD146, and von Willebrand factor; Hromada et al., 2017; Markiewicz et al., 2013). Though the pharmacokinetics of EVs remain unclear, several studies in mice have shown that therapies based on direct intravenous injection of EVs is unlikely to be very effective, due to rapid clearance of EVs from the blood stream to the liver and spleen (Smyth et al., 2015; Takahashi et al., 2013). With an estimated half-life of 1.5-3 minutes, intravenous injection with EVs is unlikely to deliver any long-term benefits (Hafiane & Daskalopoulou, 2018). Though the exact therapeutic window is unknown, it is likely to be longer than the half-life mentioned, likely falling within the range of days-weeks rather than minutes. For the purposes of this study, a therapeutic window of 14 days was assumed.

### 1.4 Hydrogels

In order to alleviate the issue of rapid clearance with injected EVs, we propose a different mechanism of EV delivery, namely through loading EVs into a hydrogel. Previous studies have shown that using a scaffold material can dramatically slow down EV clearance, improving EV-promoted tissue regeneration. For example, Zhang et al. (2018) and Zhou et al. (2019) have both attempted similar methods loading hydrogels with EVs derived from mesenchymal stem cells (using chitosan hydrogel and a matrix metalloproteinase-2 sensitive self-assembling peptide (KMP2) hydrogel respectively). Both studies found improvements in stability and EV retention as a result, as well as decreased fibrosis and promotion of angiogenesis (in treating murine hindlimb ischemia in the case of Zhang et al. (2018) and improved renal function in mice which had undergone ischemia-reperfusion injury in the case of Zhou et al. (2019).

In addition to providing more control over the release kinetics of EVs upon injection/implantation, an added advantage to delivering EVs using a hydrogel is that this hydrogel may be further enriched with cells such as cardiomyocytes and cardiac fibroblasts in order to promote cell adhesion and migration (Koti et al., 2019). These cell types could both aid in supporting tissue regeneration and contractile function following AMI, while angiogenesis is promoted by the EVs' recruitments of endothelial cells. This method is attractive as it would circumvent the need for the harvest of iPSCs and their differentiation into endothelial cells. Even so, a balance must be struck with regards to cell density within the hydrogel, as too many cells may interfere with the crosslinkability of the gel solution, therefore generating a weak gel that is too prone to degradation to adequately delay EV release (Lim et al., 2016).

For the purposes of our study, we investigated hydrogels based on methacrylated gelatine (GelMA), as well as hydrogels constructed from unmodified silk fibroin (SF) and methacrylated SF (SilkMA). These hydrogel types were selected for their promising characteristics. For example, an important consideration is that of cytotoxicity and immunogenicity. As the eventual purpose of our bioink is to promote angiogenesis and reduce fibrosis *in vivo*, the materials used should not elicit these negative effects. Both GelMA and SF-based hydrogels have been shown to exhibit low toxicity, immunogenicity, as well as good biocompatibility (for silk hydrogels this comes with the footnote that they must be produced with silk fibroin only, as the combination of silk fibroin and sericin has been found to generate a pro-inflammatory response; Spicer, 2020); and the degradation products derived from GelMA *in vivo* are generally well-tolerated peptides (Kapoor & Kundu, 2016; Tondera et al., 2016; Vettori et al., 2020). Many cell-laden hydrogels already investigated are relatively soft and prone to degradation, this seems to also be the case for GelMA. Silk-based hydrogels are proposed to have more sturdy mechanical properties due to their high protein crystallinity in the form of stable antiparallel β-sheet crystallites (formed by Gly-Ala-Gly-Ser and Gly-Ala/Ser/Tyr dipeptides; Kim et al., 2021) as well as being resistant to enzymatic degradation, which would make it more attractive for our purpose (Xiao et al., 2019).

The choice of crosslinking method is important, as this too can influence the properties of the final product. In studies where a silk fibroin hydrogel was created, oftentimes a toxic crosslinker was used to create the hydrogel (Xiao et al, 2019). For this project, we selected two methods of photo-crosslinking, namely lithium phenyl(2,4,6-trimethylbenzoyl) phosphinate (LAP) for the crosslinking of GelMA, and a combination of riboflavin and sodium persulfate (Rb/SPS) for the crosslinking of our SF hydrogel. Here, the former works through the absorption of UV-light with a wavelength around 365 nm, and the latter is initiated using concentrated visible light within the 400-450 nm range (Lim et al., 2019). The use of ruthenium (Ru) instead of riboflavin was also considered. However, previous studies done by our lab found that the addition of EVs to Ru/SPS hydrogels resulted in poor crosslinking, thus we selected riboflavin as an alternative. Although we expect to see higher cell/EV survival rates using these photo-crosslinkers, UV-light is known to be more cytotoxic than visible light, generating free radicals that are highly reactive and have a damaging effect on DNA, cells, and tissues. For this reason, it is recommended to limit exposure to UV with a wavelength of 365 nm to 27 $J/cm^3$ (ICNIRP, 2004). Hence, we expected that hydrogels generated using the Rb/SPS crosslinker

would feature a higher cell/EV survival rate than the hydrogels generated using LAP for crosslinking, in line with previous findings described by Lim et al. (2019) in their research of the effects of different photocrosslinkers on cell survival and metabolism within GelMA laden with articular chondrocytes. An added benefit of using photocrosslinkers is that they trigger crosslinking regardless of hydrogel temperature, omitting the need to heat the construct beyond temperatures tolerable to cells.

### 1.5 Mechanical properties

As the purpose of these hydrogels ideally would be to fungate as a cardiac patch, they should be able to fare well under considerable stress and must be able to withstand cyclic loading. Therefore, it must then be investigated through mechanical testing whether the construct is able to withstand these forces. Generally, a weight percentage between 0.1 and 10% polymer tends to create a gel that is sufficiently robust for the purposes of tissue regeneration while still featuring a highly porous network that allows for the exchange of oxygen and nutrients, the delivery and removal of metabolites and waste products, as well as allowing for infiltration of cells (Khan et al., 2015). In addition, high crosslink density reduces the capacity for swelling of the hydrogel, which is something to be avoided (Spicer, 2020). The swelling factor may be increased by adjusting the concentration of silk/gelatine. However, gels with a low polymer percentage, though appropriate for nutrient exchange, may be too weak to withstand the mechanical stresses presented by the cardiac environment. Hydrogels in general tend to be quite weak, so a balancing point must be found between crosslink density allowing nutrient exchange and mechanical strength when selecting the percentage of polymer in the construct.

A method to increase the construct's robustness is the addition of a supportive scaffold within the hydrogel. We investigated this through the addition of a hexagonal mesh generated through melt electrowriting, made using a printer fitted with nozzles for both MEW and pneumatic extrusion-based 3D printing. Our reasoning being that this mesh would give added tunability to the permeability and the EV/cell retention and release of the hydrogel, but most importantly a MEW mesh would significantly increase the mechanical strength and stability of our hydrogel, as hydrogels are inherently soft (de Ruijter et al., 2019). The hexagonal features of this mesh have been shown to exhibit a much larger elastic energy and greater capacity for deformation than MEW scaffolds with the more commonly fabricated rectangular microstructure. This can be considered an advantage especially when taking into account the dynamic strains the scaffold would be placed under in the rhythmic contractions of the cardiac environment. One downside to the use of this mesh is that the degradation profile of PCL, spanning several years in tissue because of an extremely slow rate of hydrolysis, would not match up with the much quicker degradation profiles of either of the hydrogels used (Spicer, 2020). We used a combined MEW/extrusion-based 3D printer (RegenHU) to generate our MEW meshes, which opens up the possibility of creating MEW meshes and extruded hydrogels with the same machine, streamlining production, reducing variability and cost.

### 1.6 EV release and uptake

As the hydrogel samples are loaded with extracellular vesicles, it is important for the hydrogel to facilitate adhesion of those items to the hydrogel itself. In the case of GelMA, as the gels origins lie in hydrolysed and denatured collagen, it inherently features many of the necessary proteins and carbohydrates naturally present in collagen which promote adhesion (such as the RGD sequence), but in the case of silk fibroin it is unclear whether this gel precursor contains these or similar proteins (Spicer, 2020; Xiao et al., 2019). Therefore, it is especially necessary to perform EV uptake and release tests. If it is found that SF is insufficiently capable of retaining EVs, the addition of synthetic peptide sequences such as RGDS (which is known to promote cell binding) should be considered (Spicer et al., 2018). Unfortunately, the scope of this project did not allow for EV uptake tests, but EV release tests were performed.

Because the hydrogel should be able to be invaded by cells, and the concentration of endothelial cell derived EVs cannot be too high to prevent inhibition of angiogenesis, it is important that the hydrogel degrade at an appropriate rate to support tissue retention. Previous research has shown that angiogenesis takes approximately 14 days on average *in vivo*, so this number was held as a baseline target for the degradation period of our hydrogel (Bejleri et al., 2018). Both SF and GelMA are biodegradable, though they have dissimilar degradation profiles, GelMA being quicker to degrade. It is expected that gradual release of EVs from hydrogels will be observed rather than a burst-release pattern, in-keeping with results found by previous research (Mol et al., 2019).

**1.7 Prepolymer solution pH**

A little-studied factor with which to influence SF-based hydrogel properties is pH. Barroso et al. (2021) developed a methacrylated silk fibroin hydrogel from a purified methacrylated-protein solution with a pH of 4.5-5, whereas pure silk solutions have a neutral pH. They found that hydrogels with pH between 5-8 for the prepolymer solution generated highly transparent, elastic, and easily manageable hydrogels. The storage and compressive moduli were significantly greater for hydrogels with pH 5 as compared to pH 7 and pH 8 hydrogels. However, this came at the expense of a significantly decreased swelling factor and increased β-sheet crystallinity (which in turn negatively affects elasticity). Overall, though pH tuning provides a way to tune physical properties of our hydrogel without adjusting polymer concentrations, we didn't make use of this fact in our study, but it is something for researchers aspiring to work with SF-based hydrogels to keep in mind.

**1.8 Degree of methacrylation**

Tuning of the physical properties of a hydrogel (i.e., porosity, pore size, stiffness, and degradability) is possible by adjusting concentration of the polymer and (photo)crosslinkers as discussed above, as well as the degree of crosslinking. This last feature, though influenced by crosslinker concentration and crosslinking period, can also be influenced by the degree of methacrylation of our GelMA and SilkMA hydrogels, which may be increased/decreased by adjusting the volume of glycidyl methacrylate (GMA) added to prepolymers. A study done by Sukul et al. (2020) found that the addition of methacryloyl groups to gelatine significantly increased pore sizes, with greatest pore sizes occurring when gelatine was 69% methacrylated. The higher the degree of methacrylation, the lower the capacity for swelling and the higher the compressive modulus (resulting in a stiffer product). In relation to cell viability, higher degrees of methacrylation correlated with higher degrees of cell attachment, and whereas cells in GelMA methacrylated at 69% did not seem to proliferate much, cells did at a degree of methacrylation of 84%. Increased degree of methacrylation also seemed to promote an initial increase in the secretion of paracrine factors, however, low degrees of methacrylation outperformed on cytokine secretion in the long run (Sukul et al., 2020). This holds true for both GelMA and SilkMA, as H. H. Kim et al. (2018) found that when methacrylation is increased, SF concentration needed to induce gelation as well as gelation time are reduced. Overall, a higher degree of methacrylation tends to lead to a stiffer hydrogel with larger pores, which may be more conducive to cell-attachment and cell proliferation. Increasing methacrylation, however, comes at the cost of reduced swelling factor and reduced cytokine secretion, as well as a slower rate of degradation (H. H. Kim et al., 2018). For the purposes of this study, GelMA and SilkMA were methacrylated to approximately 80%.

## 2. Methods:

### 2.1 Outline

The basic aim of this study is to assess the applicability of GelMA and silk fibroin-based hydrogels in the slow-release delivery of EVs via a cardiac patch, in order to promote angiogenesis and reduce cardiac fibrosis following implantation into patients who have suffered major cardiomyocyte loss due to cardiovascular diseases/events such as AMI. This EV-laden hydrogels were cell free as our focus is on delaying the release of EVs over a period of 14 days, and the addition of cells may interfere with the crosslinkability of the hydrogels, therefore affecting the stability and mechanical properties of this gel over time. However, future researchers may consider enriching such hydrogels with cardiomyocytes and cardiac fibroblasts to further promote angiogenesis. The gels created differ in prepolymer concentration and are photocrosslinked either via LAP with UV light or via the Rb/SPS system using visible light. The mechanical and rheological properties of these hydrogels were then tested, so that their effect on the release window of EVs may be ascertained. Little is currently known about the therapeutic window necessary for treatment with EVs. However, on average, angiogenesis takes place over a period of around two weeks. Thus, our initial target for the EV release window was 14 days.

### 2.2 Hydrogel preparation

Silk fibroin was isolated from *Bombyx mori* cocoons and prepared according to the procedure described by S. H. Kim et al. (2021), where 1.5 ml GMA was added after the SF was fully dissolved for batches destined to be SilkMA. Different concentrations of prepolymer solution within the hydrogels were made to ascertain their workability. For SilkMA crosslinked with LAP, concentrations of 4%, 8%, and 12% were deemed applicable, whereas for SF crosslinked via the Rb/SPS system, concentrations of 3%, 6%, and 9% were deemed applicable. Lyophilized GelMA was brought to concentrations of 3%, 6%, and 9% in PBS. Stocks were kept at 4 °C for storage. Hydrogels were crosslinked with either a final concentration of 0.1% w/v LAP in the cases of GelMA and SilkMA, or 2/10 mM Rb/SPS in the case of SF. Photocuration periods for GelMA and SilkMA were 10 minutes sans EVs. Photocuration periods for SF hydrogels and all EV-loaded hydrogels were 25 minutes, as the addition of EVs to GelMA was observed to affect the necessary time needed for crosslinking. GelMA and SF groups were assessed for their mechanical and rheological properties, static and dynamic EV release kinetics. Hydrogel samples were cast by depositing 52 μL of solution in a 2 mm thick Teflon mould with 6 mm wells. SF + Rb/SPS was photo-crosslinked through visible light using a 50Hz 20W LED floodlight, whereas SilkMA + LAP and GelMA + LAP were photocrosslinked using a 4W hydrozone lamp producing UV light with a 365nm wavelength.

Initially, we had planned to compare GelMA to methacrylated SF (SilkMA). However, the addition of glycidyl methacrylate (GMA) to the SF resulted in inconsistent results during the dialysis process, sometimes causing the gel precursor solution to prematurely gelate within the dialysis tubes. Therefore, the SilkMA avenue was abandoned in favour of SF that wasn't treated with GMA, yielding much more reliable batches of gel precursor solution. The few results that were obtained using successful SilkMA batches have been included in this paper.

Silk fibroin sterilisation is challenging. Silk fibroin solutions, when cocoons are boiled for five minutes, contain strands that are too long to be sterilised by filtration, and sterilisation with heat, steam, or alcohol is not feasible as these factors cause gelation. Thus, all silk fibroin solutions were sterilised through 30 minutes of exposure to UV in a UV oven (prior to the addition of photocrosslinkers to avoid premature gelation).

The degree of methacrylation (DM) of GelMA was quantified by colleagues from the RMCU through proton nuclear magnetic resonance spectroscopy ($^1$H NMR). The DM was calculated from the integrated area of signals corresponding to the lysine methylene groups (δ = 7.05 – 7.25 ppm) and the phenylalanine groups of gelatine (δ = 2.82 – 2.91 ppm), in line with the method previously reported by Gu et al. (2021). DM was determined to be approximately ~83% using the following formula:

$$\mathrm{DM}(\%) = 1 - \frac{Peak\ area(lysine\ methylene)}{Peak\ area(phenylalanine)} * 100 \quad (1)$$

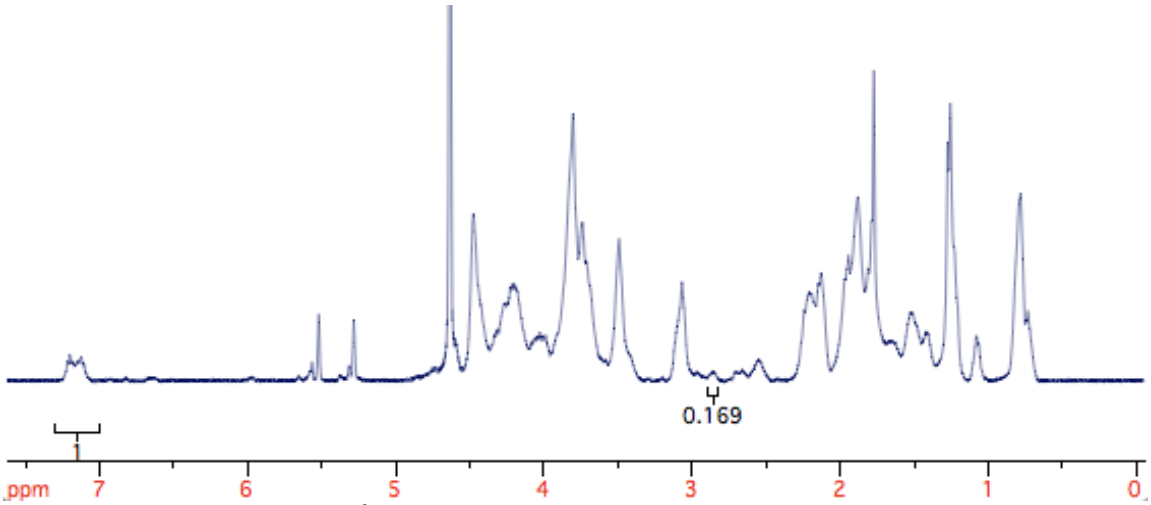


***Figure 1.*** *typical results from [1]H NMR testing of GelMA, with peaks for lysine methylene and phenylalanine denoted in the graph (0.169 and 1 respectively), accounting for a degree of methacrylation of approximately 83.1%.*

**2.3 Extracellular vesicle preparation**

Extracellular vesicles obtained from human induced pluripotent stem cells (hiPSC) in Portugal by Professor Margarida Serra's research group in IBET in Lisbon, Portugal, according to protocols previously described by Louro et al. (2022). hiPSCs were first cultured and expanded on Matrigel-coated plates at 37 °C, and then differentiated towards cardiomyocytes (CM). When over 80% of the cultured cells exhibited beating (and had thus differentiated towards cardiomyocytes), cells were dissociated from the coated plates, to create hiPSC-CM aggregates. hiPSC-CM aggregates were matured under influence of maturation medium, and cells were harvested at different time points to assess cell viability. From the matured hiPSC-CM cell aggregates, EVs were separated through differential centrifugation and subsequently through density gradient ultracentrifugation. EVs were then obtained by removing the resulting supernatant, and a stock solution was created by adding a homogenization buffer. EV concentrations of the EV-buffer stock solutions were then determined through nanoparticle tracking analysis (NTA) by IBET, and fluorescently labelled with PKH26. EVs were then shipped to the RMCU, where they were added to our hydrogel precursor solution at an initial concentration of $1.50*10^{10}$ particles/ml of hydrogel solution.

**2.4 Degree of methacrylation**

Degree of methacrylation may be analysed through Fourier-transform infrared spectroscopy (FT-IR), proton nuclear magnetic resonance ($^1$H-NMR) spectroscopy, or through a 2,4,6-trinitrobenzene sulfonic acid (TNBS) assay (S. H. Kim et al., 2021). For the purposes of our study, all GelMA and SilkMA hydrogels used a concentration of 0.8 MA per gram of gelatine/SF for a degree of functionalization of ~80%. The DM of the GelMA used for this study was determined through $^1$H-NMR, where spectra were obtained through the usage of an Agilent spectrometer (400 MHz). Freeze-dried GelMA was allowed to reach room temperature in a closed container, after which 5 mg GelMA was dissolved in 800 µl of deuterium oxide inside an NMR glass tube. The mixture was kept at a consistent 37 ºC until it had homogenised. 64 scans in the 0-12ppm range were recorded in order to generate spectra, which were then subsequently analysed with iNMR software.

**2.5 Photoinitiator concentration**

Altering the concentration of the photocrosslinker has an effect on crosslinking time, viscosity, and cell viability. In addition, Born et al. (2021) mentioned in their preprint that they found that increasing photoinitiator concentration prolonged the EV-release window.

Lowering the concentration of the photocrosslinker, on the other hand, increases the time necessary to crosslink, thus increasing exposure of any cells in the hydrogel to damaging UV light. The recommended final concentration of LAP is between 0.05 – 1.0% w/v (Monteiro et al., 2018). Thus, a LAP concentration of 0.1% w/v was assessed using hydrogels with the previously mentioned gelatine/silk concentrations.

Lim et al. (2019) found that the optimal concentration of Ru/SPS, based on crosslinking time and desired mechanical properties, was 0.2/3 mM when exposing 10% w/v GelMA for 3 minutes. However, the optimal exposure time is highly dependent on light intensity, and thus the periods stated may not be appropriate for our experiments. They note that the usage of Ru/SPS is superior to the use of LAP as it requires much lower concentrations and is therefore likely less harmful cells, as well as being less disruptive of the hydrogel's mechanical and rheological properties. Concentrations investigated by Lim et al. (2019) were 0.1/1, 0.2/2 and 0.3/3 of Ru/SPS (mM/mM) and 0.05% w/v LAP, both at exposure durations of 0.5, 1, 3, 5, 10, and 15 minutes. At 0.1/1 mM/mM Ru/SPS, 5 minutes were necessary to make a stable hydrogel with a sol fraction between 35-42%. At 0.2/2 mM/mM Ru/SPS, there is a significant decrease in crosslinking time (0.5 min) to obtain a similar sol fraction (30%). Increasing linkage time eventually led to a plateau in the sol fraction to about 15%. Sol fractions when using Ru/SPS were identical between 0.2/2 mM/mM and 0.3/3 mM/mM concentrations. From results of printing with Ru/SPS in our lab, a concentration of 0.5/5 mM seems to generate hydrogels with superior mechanical strength. Overall, LAP was faster to crosslink, showing a plateauing sol fraction after 0.5 minutes of UV exposure. This is in contrast to results found by Yang et al. (2021), where the Ru/SPS system was found to have the greatest crosslinking speed, requiring less than 5 seconds to polymerize. Part of the difference in photoinitiator performance between these studies may well be attributed to the utilisation of different hydrogels (GelMA vs GelAGE). However, the addition of EVs to hydrogels containing Ru/SPS was found to cause the hydrogel to fail to crosslink completely, therefore, this avenue of photocuration was eventually abandoned. Instead, we investigated SilkMA and GelMA crosslinked with 0.1% LAP, as this has been shown to be an appropriate concentration for the formation of stable hydrogels. A concentration of 2/10 mM Rb/SPS was used for the crosslinking of SF, as this concentration has been shown to produce stable SF hydrogels (Piluso et al., 2020).

### 2.6 MEW mesh

Gels were either tested with or without the addition of a melt electrowritten (MEW) polyester polycaprolactone (PCL) mesh, added with the intention of providing extra stability and mechanical strength to the construct and to tune the EV release kinetics. These meshes featured a hexagonal structure of fibres with a diameter of around 13 µm, and it were generated in the manner described by Castilho et al. (2018). Granular medical grade PCL was inserted into a glass syringe and molten at 85-90 ºC. The PCL was subjected to pressurized $N_2$ via a sealed hose. The polymer filament was then subjected to high voltage and deposited in wavy connecting lines, creating a hexagonal pattern. A hexagonal structure is chosen for its added stability and strength. Meshes were generated in rectangular sheets of 35 layers of PCL, upon which 5mm circles were created using a biopsy punch (depending on whether the gels had a diameter of 6mm. When this scaffold was added in our casted hydrogels, half of the solution was added before placing the mesh into the mould, finishing with the other half of the solution so that the mesh is fully immersed in the hydrogel solution. Mechanical, rheological, and EV-release tests were conducted on gels with and without meshes, whereas hydrogel formation and degradation kinetics tests utilised only gels without meshes.

### 2.7 Hydrogel formation test

In order to assess the formation of the different hydrogels, 3 different factors were assessed, namely: sol fraction, actual macromer fraction (AMF), and swelling factor. The sol fraction denotes the fraction of prepolymer solution added that is actually crosslinked, as opposed to the prepolymer solutions that remains soluble after being exposed to the relevant light source. Sol fraction is calculated through the following equation (1):

$$Sol\ fraction = \frac{dry(t=0) - dry(t=1)}{dry(t=0)} \quad (2)$$

In order to assess the Sol fraction, hydrogels without meshes and EVs were cast in Teflon moulds with circular wells with a diameter of 6mm and a height of 2mm. Gels were then weighed and either freeze-dried immediately or incubated at 37 ºC in 500 µl PBS for 24 hours and then freeze-dried by first freezing the samples overnight and then lyophilizing for 3 days. These weights were also used to assess the swelling factor and actual macromer fraction, where the swelling factor denotes the hydrogel's swelling capacity in PBS after a 24-hour period, and the actual macromer fraction denotes what fraction of the wet weight of a hydrogel is polymer (as opposed to water). These were calculated according to equations (2) and (3):

$$Swelling\ factor = \frac{wet(t=1) - dry(t=1)}{dry(t=1)} \quad (3)$$

$$AMF = \frac{dry(t=0)}{wet(t=0)} \quad (4)$$

Ordinary one-way ANOVAs with multiple comparisons were then performed per gel-type (GelMA, SF, and SilkMA) for the Sol fraction, swelling factor, and AMF.

**2.8 Degradation kinetics test**

A degradation kinetics test was performed by casting 5 mm by 2 mm hydrogel disks in a sterile environment. Hydrogels were made without EVs or meshes, and degradation kinetics tests were performed for GelMA and SilkMA crosslinked through UV with LAP for 10 minutes, and SF crosslinked through concentrated visible light with Rb/SPS for 25 minutes. Samples were weighed, then suspended in 1ml of PBS, after which they were left to degrade in a 37 ºC incubator for the selected time periods (1, 2, 4, 7, 14, 21, and 28 days). For each batch of gel, 3 samples were kept separate and immediately weighed and freeze-dried to ascertain the actual macromer fraction. After the degradation period had passed, PBS was removed from the Eppendorf and the hydrogel disk was freeze-dried and weighed. Dry weight at t=t and the relevant actual macromer fraction were used to calculate the dry weight of the sample at t=0 and compared to t=t in order to assess the rate of degradation. Degradation was defined as the % loss of dry mass, which consists mainly of the polymer part of the hydrogel and less so of the photoinitiator. This was calculated using the following formula:

$$\%\ degradation = 100 * \frac{dry(t=0) - dry(t=t)}{dry(t=0)} = 100 * \frac{(wet(t=0) * AMF) - dry(t=t)}{wet(t=0) * AMF} \quad (5)$$

A two-way ANOVA with multiple comparisons was subsequently performed for all degradation kinetics tests, where p = 0.05.

**2.9 EV release (fluorimetry and nanoparticle tracking analysis)**

In order to assess the EV release window from our gels, an EV release test was performed. Sterile GelMA + LAP and SF + Rb/SPS samples with and without EVs and meshes were cast (n=3 per condition). Samples were transferred to individual Eppendorf tubes with 500 µl sterile PBS. At pre-selected time points (GelMA: 4h, 1d, 2d, 4d, 7, & 14d; SF: 4h, 1d, 3d, 7d, & 14d), 250 µl fluid was removed per Eppendorf and frozen, while 250 µl sterile PBS was added to the samples to keep the volume into which EVs could release constant. Fluids were then transferred to a 96-well plate (250 µl per well) and analysed using a Multimode plate-reader detecting PKH26, EV concentrations were determined by comparing fluorescence to an EV standard curve made in the same well plate with known concentrations. Before these tests were done, it was determined whether our photoinitiators could cause interference. For LAP, it was already known that this photoinitiator caused little to no interference when detecting PKH26, but for Riboflavin there was some uncertainty. Thus, a standard curve with known concentrations of Rb was made and analysed. Unfortunately, when detecting fluorescence of wavelengths 520±8-567±8 nm riboflavin generated a significant amount of noise. Thus, for the actual EV release tests, well plates with SF + Rb/SPS always contained samples with and without EVs so that an estimate of noise generated by the riboflavin may be made and subtracted from the values of EV-loaded samples. Cumulative and individual EV-release was then calculated per time-point, accounting for dilution through the following formulae:

$$Individual\ EV\ release\ (t=t) = 100 * \frac{number\ of\ EVs\ (t=t) + 0.5 * number\ of\ EVs(t=t-1)}{EV\ load} \quad (6)$$

$$Cumulative\ EV\ release\ (t=t) = Individual\ EV\ release\ (t=t) + Cumulative\ EV\ release\ (t=t-1) \quad (7)$$

Where EV load is always 1.50E+10 particles/ml, and the number of EVs is calculated by first generating a trendline for the EV standard curve, and then inputting sample fluorescence into the generated equation for that trendline. For SF gels, an additional step is necessary in calculating the number of EVs, where the average fluorescence of samples without EVs matching other conditions of the relevant sample is subtracted to account for Rb interference before calculating the true number of EVs. Sadly, even with these steps taken to correct for Rb interference, it was deemed impossible to accurately gain EV counts from SF samples through fluorescent plate reading. Thus, EV counts were instead garnered through nanoparticle tracking analysis (NTA) using a NanoSight NS300 machine. 5 captures of 60 seconds each were taken in triplicate per condition using standard measurements, with initial screen gain set to 4.0 and camera level set to 9. For processing, screen gain was set to 5.0, and detection threshold was set to 26. Two-way ANOVAs were performed on EV release data from GelMA and SF with and without meshes in GraphPad Prism on both cumulative and individual (EV release per time point) data. Time points were 4 hours, 1 day, 2 days, 4 days, 7 days, and 14 days.

The NanoSight's own software calculated mean and standard error for particle concentration for each test. Since each test contained the same number of captures (N=5), measurements done in triplicate were averaged according to the following equations:

$$\mu_{combined} = \frac{1}{3}(\mu_1 + \mu_2 + \mu_3) \quad (8)$$

$$\sigma_{combined} = \sqrt{\frac{(SE_1 * \sqrt{5})^2 + (SE_2 * \sqrt{5})^2 + (SE_3 * \sqrt{5})^2}{3}} \quad (9)$$

$$SE_{combined} = \frac{\sigma_{combined}}{\sqrt{3}} \quad (10)$$

## 2.10 Dynamic EV release

A dynamic EV release test was performed using an MTS Criterion universal testing machine fitted with a parallel plate system and a 50N sensor. 6x2mm SF hydrogel discs were placed into a 2mL PBS bath (consisting of 3D printed PLA generated with an Ultimaker S3) and subjected to cyclic loading with a frequency of 1 Hz at a maximum strain of 10% to simulate cardiac compression. This was done in order to investigate whether the dynamic environment of the heart might affect the EV release window. Due to time and material constraints this test was limited to SF + Rb/SPS gels with and without meshes, as these are the focus of our research. As a control, half of the gels (n=3 per condition) were placed in the PBS bath but not subjected to cyclic loading. After a 15-minute period of cyclic loading, the PBS was removed from the bath, transferred to an Eppendorf tube and frozen. The water bath was then emptied, rinsed with PBS, dried, and re-used. PBS samples were analysed through NTA with a NanoSight NS300 machine in order to ascertain the level of EV release. All NanoSight settings were identical to those used for the EV release test described in the previous section, generating 5 captures of 60 seconds in triplicate per condition. As with the EV release test described in 2.9, measurements done in triplicate were averaged according to formulae 7-9. Data was analysed using GraphPad Prism through ordinary two-way ANOVAs.

## 2.11 Mechanical and rheological properties

### *2.11.1 Compression*

Unconfined compression tests were performed using an MTS Criterion universal testing machine fitted with a parallel plate system and a sensor with a maximum capacity of 50N. Compression tests were run using 6 x 2 mm cylindrical cast hydrogels which were deformed to a maximum strain of 85% at a speed of 0.003 mm/s. Hydrogel samples were cast at the RMCU in Utrecht, then transported to a TU/e lab in Eindhoven for overnight storage at 4 ºC, before being used for testing. Tests were performed with between 3 and 6 replicates for each condition.

Data gathered from compression tests conducted as described in the methods section were analysed in R, outliers were removed, and Young's moduli and yield strengths were calculated. In order to obtain yield strength, a function was created which generated linear models over the data per replicate, varying endpoints of the linear models from 1% to 85% strain (the cut-off strain for our compression tests) in steps of 0.1%. The function then selects the linear model with the highest r squared (the best fit). The function then defines the yield point/strength as the stress value corresponding to the measured strain value which is closest to the endpoint which generated the highest r squared. Young's moduli can then be derived as the coefficient of the linear model with the highest r squared.

After Young's moduli and yield strength were collected for each replicate per gel type with and without mesh, groups were compared using Student's T-tests.

### *2.11.2 Stress-relaxation*

Unconfined stress-relaxation tests was performed using an MTS Criterion universal testing machine fitted with a parallel plate system and a sensor with a maximum capacity of 50N. Hydrogel samples were transported identically to those used for the compression tests. Stress relaxation tests were run using 6 x 2 mm cylindrical cast hydrogels, generating 6 replicates for each condition. Hydrogels were tested while submerged in PBS. Following a 0.1 N pre-load, hydrogel samples were subjected to a strain ramp with a maximum strain of 15%, ramping up at 0.01 mm/s. After 15% strain was reached, strain was kept constant for 15 minutes and changes in force were measured. $\tau_{1/2}$, which was defined as the time it took after reaching 14.9% strain (defined as t=0) to halve the stress found at t=0, was calculated from our data by finding the intercept of the average stress at t=0 per gel type x 0.5 with each replicate's stress-time curve in RStudio. As our data contains a lot of noise due to the low loads measured as compared to the sensitivity of the sensor used, we elected to clean our data by making calculations over a rolling mean with window-size 25. This window-size was selected as it removes outliers and reduces variation without compromising too much on reliability of our data.

*2.11.3 Amplitude sweep*

Amplitude sweeps were conducted using TA Instruments' Discovery HR-2 rheometer fitted with 20mm parallel aluminium plate geometry. Temperature of the hydrogel was kept at a constant 20 ºC with the help of a Peltier plate. Data was acquired through TRIOS software. Hydrogel samples were cast as 6 x 2 mm cylindrical discs, and 6 replicates were generated for each condition (gel type, concentration, and mesh presence). Frequency was kept constant at 1 Hz, while strain was increased to a maximum of 1500%. Graphs were generated and data was analysed in RStudio, outliers were removed, resulting in 3-6 samples per group.

*2.11.4 Frequency sweep*

Frequency sweeps were conducted using TA Instruments' Discovery HR-2 rheometer fitted with 20mm parallel aluminium plate geometry. Temperature of the hydrogel was kept at a constant 20 ºC with the help of a Peltier plate. Data was acquired through TRIOS software. Using data from the amplitude sweeps and compression tests, 1% strain was deemed appropriate for the frequency sweeps, while frequency was increased to a maximum of 15Hz. Hydrogel samples were cast as 6 x 2 mm cylindrical discs, and 6 replicates were generated for each condition (gel type, concentration, and mesh presence), however, only on average half of those replicates yielded usable results. Graphs were generated and data was analysed in RStudio, outliers were removed, resulting in 3-6 samples per group.

## 3. Results and discussion:

### 3.1 Hydrogel formation:

No significant differences were found between Sol fractions, likely due to high variance, as can be derived from figure 2.A. Even so, it seems that higher concentrations result in a lower Sol fraction for silk-based hydrogels, whereas Sol fraction increases with higher polymer concentration for GelMA. This may suggest that low concentrations of GelMA and higher concentrations of silk-based hydrogels require less time to photo-crosslink fully. The reliability of the results obtained are dubious however, as significant differences in Sol fractions dependent on gel concentration have been observed in past research and were thus expected. The high variance observed in our samples is likely due in part to scale inaccuracies, as sample weights were very small, testing the limitations of the supposedly microgram-accurate scales. In order to alleviate this issue, samples were weighed thrice, and average weight was noted. In addition, hydrogel formation tests were done with 3 x 52µl hydrogel discs per Eppendorf tube. However, this increase in sample weight may not have been enough to produce reliable scale results. In future, heftier samples should be used (or more 52µl hydrogel discs) to reduce the effect of scale inaccuracies.

For the swelling factor, the only significant differences were found between different concentrations of SF, whereas GelMA and SilkMA of different concentrations showed no significant difference. Mean swelling factor for the different concentrations of SF ranged from 5.985 to 18.56, whereas GelMA and SilkMA ranged from 9.718 to 11.15 and from 11.31 to 13.85 respectively. For all gels, however, a higher concentration of polymer seemed to result in a lower swelling factor. This makes sense, as an increase of polymer concentration increases the number and density of crosslinks within the hydrogel, negatively affecting the gel's ability to take up water. In the case of GelMA, the lack of difference in swelling factors according to polymer concentration may be due to the increase in Sol fraction at higher concentrations, which may indicate that a higher percentage of polymer did not crosslink/gelate. Therefore, the crosslink density in the higher concentrations of GelMA would not be as high as expected and the higher concentrations of GelMA would not affect the swelling factor as much as anticipated.

As for the actual macromer fraction, the only significant difference found between gels of different concentrations was between GelMA_3% and GelMA_12%, with means ranging from 0.0623 to 0.1109.

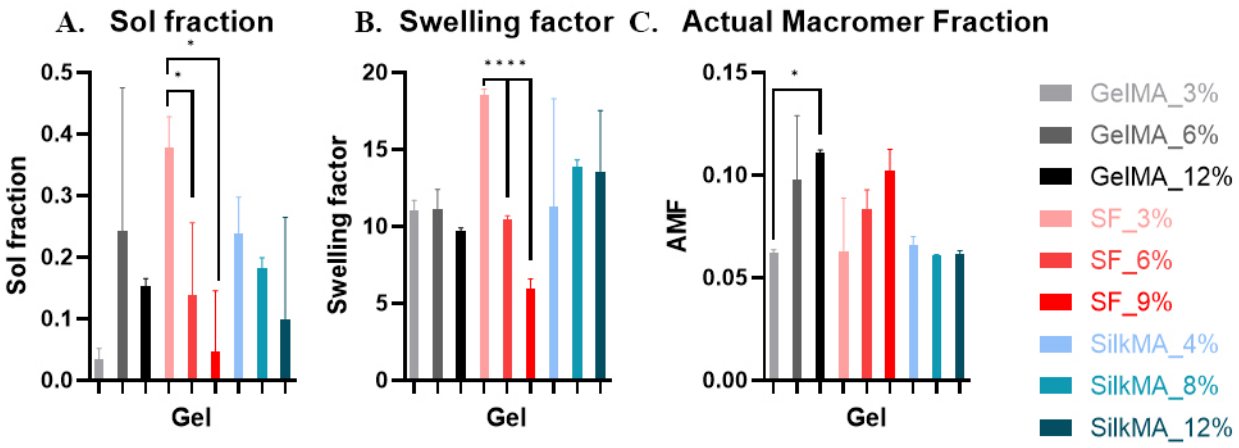


***Figure 2.*** *hydrogel formation tests conducted on EV-less, mesh-less gels: sol fraction (A), swelling factor (B), and actual macromer fraction (C) are noted as ratios on the y-axis, while different gel types are denoted as coloured bars. Significance in factor between gel concentrations of the same hydrogel type (GelMA, SF, and SilkMA) is denoted with asterisks.*

**3.2 Degradation kinetics:**

Relatively few of the comparisons were statistically significant, likely in part due to the high variability between replicates, which can be seen in figure 3.A-I. This may be due to a number of factors including the difficulty of obtaining accurate and consistent results when weighing due to the very slight weight of the samples (hence the decision to add 3 x 52µl samples per Eppendorf as opposed to the initial 1 sample), as well as human error due to inexperience. In addition, the scales may not be consistent over time. Samples dry weights$_{t=t}$ were noted on the day those samples finished freeze-drying rather than weighing all samples together, which may have yielded more variation due to inconsistencies in the scale used over time (in particular, the unexpectedly high degradation of SilkMA samples on day 4 jumps out). Regardless, an indication of degradation over time can certainly be observed through the scatter plots in figure 3. Although most comparisons did not yield a significant result due to the high variability, by day 21, the difference between GelMA_3% and the silk-based hydrogels is so stark that even though there is high variability, a significant difference is observed. In addition, from day 21 onwards, GelMA_3% also shows a significantly higher degradation than higher concentrations of GelMA. By day 28, there is also a significant difference in degradation between GelMA_12% and both SilkMA_8% as well as SilkMA_12%, where GelMA_12% has lost a higher percentage of its dry mass. For more info on which comparisons generated significant results, see supplementary table 1. It seems likely then, that GelMA_3% is unfit for the purposes of prolonged EV release, as hydrogels of this concentration do not seem to last much longer than 4 days, whereas we are aiming for a release window of 14 days. The concentration of hydrogel precursor seems to have a significant effect on GelMA hydrogels, and less so for SF-based hydrogels. Whereas GelMA_3% reached complete degradation by day 4, GelMA_6% and GelMA_12% reached a mean degradation of 45.34% and 39.65% by day 28 respectively. Silk-based hydrogels, on the other hand, all reached an end mean degradation below 25%, and thus seem to be more stable over time than GelMA. As we hope to achieve a relatively consistent rate of EV release over our 14-day release window, the superior stability of silk-based hydrogels are expected to make them a more attractive choice over GelMA for our purposes. Although significant differences were not found in many instances, they are also not necessarily expected in all groups. The high degradation of GelMA_3% as compared to the degradation of higher concentrations of GelMA is to be expected, as these gels were observed to be much weaker and more challenging to get to crosslink successfully. Proportionally, gels made at a concentration of 3% GelMA are mostly water, even more so than the higher concentrations of GelMA. Because of this, and the subsequent difficulties in crosslinking, these crosslinks may also fail more easily over time than with GelMA hydrogels at higher concentrations. For GelMA_6% this seems to not be the case, perhaps the presence of GelMA in these hydrogels has reached a point at which crosslinks are more prevalent, stable, and thus more difficult to break and less prone to degradation over time. If so, then a reduction in degradation as a result of increasing the percentage of GelMA beyond 6% would not be expected. SF-based gels have been shown to have higher mechanical strength, and thus may not need as high a concentration of hydrogel precursor solution as GelMA due to the strength of their bonds. It is then unsurprising that raising SF or SilkMA concentration does not result in significantly reduced degradation, especially since degradation of SF and SilkMA at the lowest concentrations investigated is already fairly low.

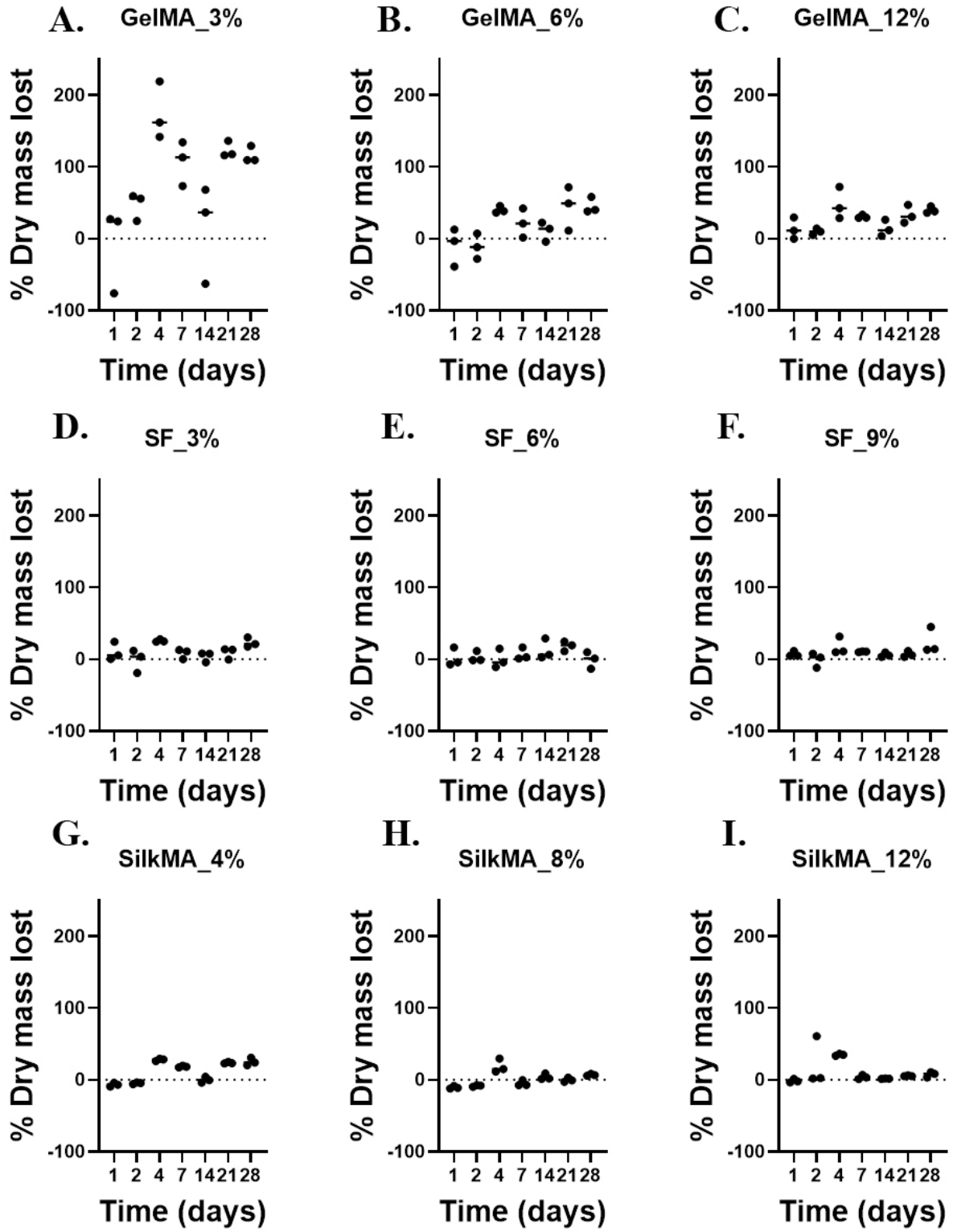


***Figure 3.*** *Degradation of all different gels tested over time, separated by gel-type and concentration. None of these gels contained either EVs or meshes. A-C show data from GelMA hydrogels, D-F show data from SF gels, and SilkMA data is shown in G-I. Mean values are indicated with a dash. From these graphs we can see that GelMA degrades much quicker than silk-based hydrogels, approaching 100% degradation whereas silk-based hydrogel degradation tends to stay below 40% even by day 28.*

### 3.3 EV release:

*3.3.1 Fluorescent microplate reading:*

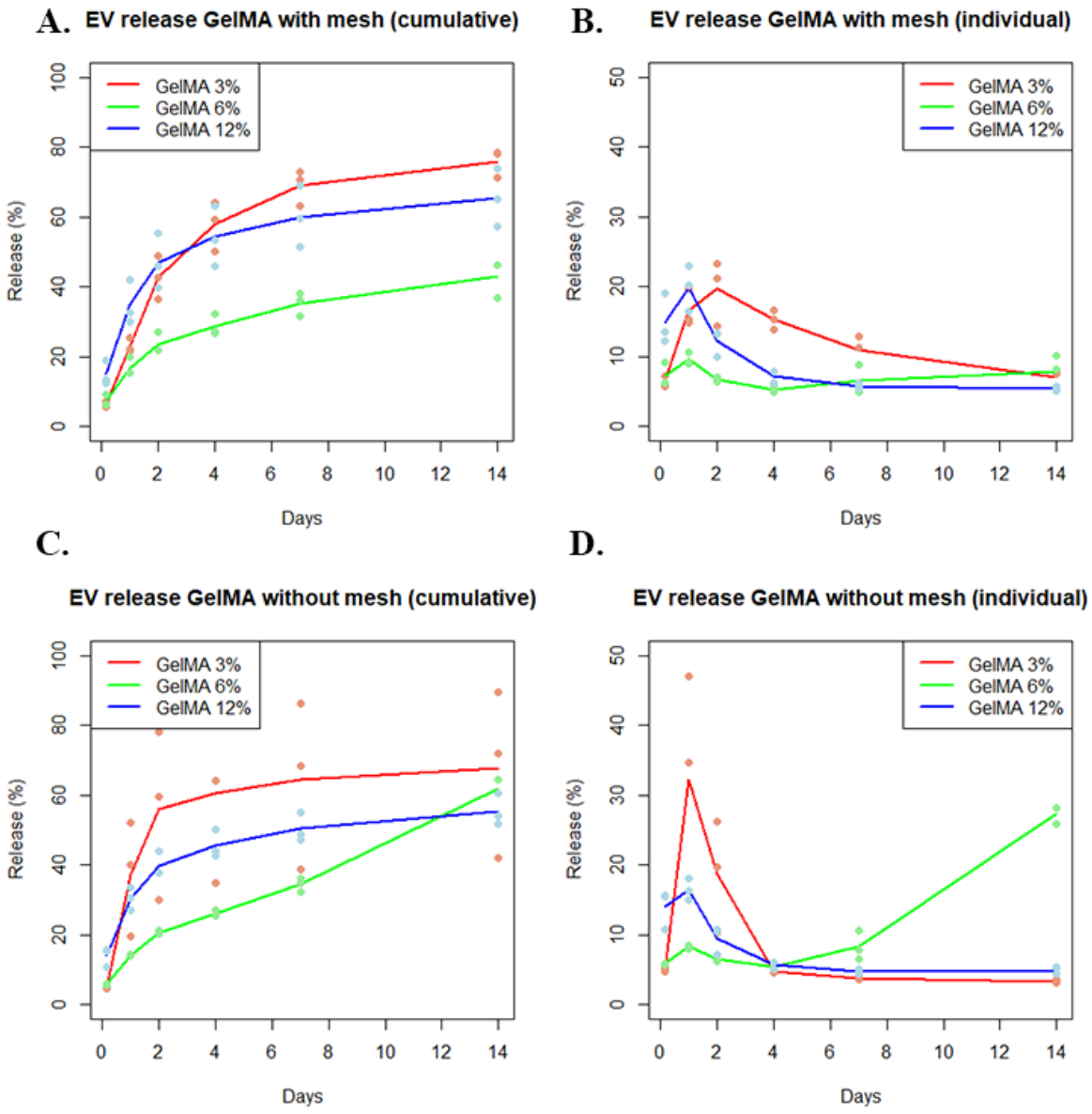


***Figure 4.*** *Cumulative (A&C) and individual (B&D) release of EVs from GelMA with (A&B) and without (C&D) meshes over a period of 14 days. Graphs B and D show that there is a peak in EV release within the first 4 days, after which (except for GelMA6% without mesh) EV release reduces over time. From graphs A and C, we gather that the addition of a mesh seems to increase EV release somewhat for GelMA 3% and 12%.*

ANOVA results suggested that the effects of mesh addition on EV release are limited, as the only significant differences in individual releases due to the addition of a mesh were found for GelMA_3% on days 1 and 2 (when looking at individual release figures per time point, not when looking at cumulative release), and for GelMA_6% on day 14 (individual release). For all three occurrences where mesh addition had a significant effect, EV release was higher in gels without meshes. Gel precursor concentration, on the other hand, seemed to have a more extensive effect on EV release patterns, as significant differences were found between the three concentrations for most

time points, especially so when raising GelMA concentration from 3% to 6%. For all groups (with the exception of GelMA_6% without mesh), individual release was highest on day 1 or 2 and decreased to between 3% and 7% EV release per day at day 14. The marked increase in release for GelMA_6% at day 14 (and less so at day 7) seems unusual and may be a product of some error in the preparation of the microplate analysed. In general, although all concentrations of GelMA showed a peak of EV release within the first week, increasing GelMA concentration seemed to produce a gel that released EVs consistently more rapidly than low concentration gels, as individual EV release stabilised more rapidly. In terms of reducing burst-release of EVs, it seems that GelMA_6% performs best. More info on which comparisons between groups yielded significant results can be found in supplementary tables 2.A and 2.B, which show results on ordinary two-way ANOVAs for both data from individual and cumulative EV release.

Previous research suggests that high stiffness may increase EV release, especially when also featuring stress relaxation, regardless of hydrogel degradation (Lenzini et al., 2020). It is thus expected that there is a play-off between degradation, stiffness, and stress relaxation in reaching optimal EV release patterns. This may explain why, for both highest and lowest concentration GelMA hydrogels, EV release is higher than the medium concentration. From the degradation kinetics test in section 3.2 we found that degradation is significantly higher in GelMA 3%, and from the amplitude sweep in section 3.4.3 and stress-relaxation test in section 3.4.2 we found that all gels exhibited stress-relaxation (which is due to the physical nature of the crosslinks in the hydrogel rather than covalent bonds) and higher concentrations of hydrogel led to increased stiffness as well as shortened relaxation periods. It is thus likely that with GelMA 6%, a compromise is reached between EV release through hydrogel degradation, and EV release through permeability caused by stress relaxation behaviour and stiffness, therefore exhibiting the lowest degree of EV release overall.

*3.3.2 Riboflavin interference:*

Prior to EV release testing, a standard curve with known concentrations of Rb was generated to indicate whether Riboflavin would cause interference during the actual EV release test. If all riboflavin in a hydrogel sample were to leech into a fluid sample destined for plate reading through fluorescence, this fluid would have a Rb concentration of 0.416 mM. At 0.416 mM, the influence of Riboflavin to fluorescence in the wavelength-range exhibited by PKH26 is in the order of $\pm 8*10^4$. The fluorescence exhibited by fluid containing EVs at a concentration representative of 100% release from a hydrogel sample, on the other hand, is in the order of $\pm 1*10^4$. Due to this fact, it was expected that the addition of Riboflavin to SF gels would cause considerable noise, and therefore samples without EVs (but with Rb) were assessed alongside samples with EVs to account for noise caused by Riboflavin. However, the influence of Rb was seen to be so extensive that it was found to be impossible to accurately ascertain EV counts from amongst the noise. Therefore, EV release samples for SF hydrogels were saved and instead assessed via nanoparticle tracking analysis (NTA).

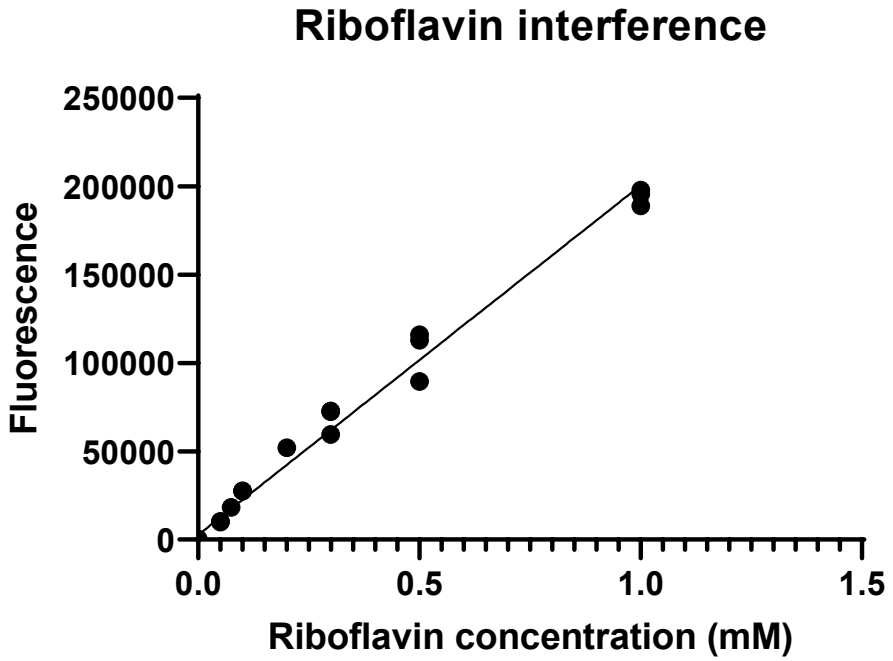


***Figure 5.*** *Riboflavin fluorimetry standard curve generated to ascertain influence on EV release tests with Rb-containing hydrogels via fluorimetry. Fluorimetry settings were tuned to excitation and emission values expected from our PKH26-affixed EVs. The graph indicates a great deal of interference due to Rb presence.*

*3.3.3 Nanoparticle tracking analysis:*

ANOVA results on particle diameter size comparisons between samples with and without EVs yielded no significant results, suggesting that particles released from samples without EVs followed a similar size distribution to particles released from samples with EVs. Particle diameters were all mostly in the range expected according to the EV size distribution found by our colleagues in Portugal, which were also analysed through NTA (for reference, the particle size distribution we found for groups without EVs was 235.3 ± 122.6 nm, for groups with EVs it was 207.1 ± 87.4 nm, and for the particles analysed by the Portugal group it was 195.4 ± 62.8 nm). There were also no significant differences found in particle diameter between groups with or without meshes, suggesting that the diameter of the hexagons in the meshes' hexagonal microstructure was not so small as to limit the release of particles at the higher end of the range of diameters found in groups without meshes.

Oddly enough, although gradual particle release was found in groups containing EVs, large numbers of particles were also released in control groups that weren't supposed to contain EVs (see figure 6 and supplementary figure 1). This is unexpected, especially in light of the results from the EV dynamic release experiment described in section 3.3.4, where particle release was lower in groups without EVs. Multiple theories could be devised as to why this may have occurred, but it is unsure which if any is the case. For one, samples in this test were rescued from microwell plates in our initial experiment with fluorescent microscopy described in section 3.3.1, meaning that these samples experienced more exposure to light and room temperatures than GelMA samples from the fluorescent microscopy EV release study. In addition, samples went through an extra freeze-thaw cycle, which may have caused bursting of a portion of the EVs. These factors may have caused figures of particle

release to be closer together between EV and blank groups. However, this does not account for the unexpectedly high number of particles in the blank groups. This may have been a result of contamination. Although the risk of contamination was quite low as samples spent most of their time in closed Eppendorf tubes, and the only times where Eppendorf tubes were opened, and fluid samples were taken were done in the sterile environment of a flow hood in an ML-2 lab. However, since hydrogels spent a maximum of 14 days in a 37 ºC incubator, it is not unreasonable to think that a contamination might have occurred, and the contaminating particles may have proliferated in the incubator. One way in which contamination might have occurred, and this seems reasonable considering that particle release from blank groups is unexpectedly high from the first time point onwards, is that one or more of the ingredients used in hydrogel formation was insufficiently sterilised. A likely candidate is the silk fibroin itself, as finding a way to sterilise this material has been challenging throughout this study, and although the solution was sterilised by UV exposure for 30 minutes, this may have been insufficient in this case. Even so, from NTA videos it was unclear what type of particles these might then have been since all particles viewed were similarly round in shape. Were it a contamination with some sort of bacteria, this might have been deduced if we had seen rod-shaped particles in addition to the expected spherical particles, for example.

Even in light of this unfortunate circumstance, we can see from the graphs in figure 6 and supplemental figure 1 that there are slight differences in release patterns (for more information about which comparisons yielded significant differences through ANOVA testing, see supplemental figures 3.A-C. For one, particle release patterns in blank groups were much more similar between groups than particle release patterns in groups containing EVs, where differences were much more pronounced. In addition, there are differences in particle release from SF_3% with meshes between blank and EV groups, where blank groups released particles at a consistent rate whereas the EV groups resulted in significant differences in release from timepoint to timepoint (see figure 6.B). This group also released a substantial number of particles more for groups with EVs than without EVs, suggesting that EVs make up a large amount of this difference. There is also a significant peak in particle release that can be observed in SF_9% without meshes on day 7, which is absent from the group without EVs. This is promising, as bacteria are expected to have different release patterns from hydrogels than EVs. EV groups consistently showed that high concentrations of hydrogel resulted in an increase in particle release, which holds with our results from EV release studies from GelMA (where the medium concentration resulted in the lowest EV release). In addition, all SF groups that did not contain a mesh resulted in a very slightly increased particle release, although this difference was only considered significant for SF_3% with EVs at 4 hours. Different to our results from the EV release study in GelMA, the medium concentration did not result in the lowest degree of particle release. Instead, particle release was lowest for the lowest concentration of SF and increased monotonically with an increase in hydrogel concentration. Whereas most GelMA groups showed a large peak in EV release around day 1, this peak was delayed in SF groups to day 3 for all groups except SF_9% without mesh (which showed a peak at day 7). To add to this, with an exception for GelMA_3% without meshes, GelMA seemed to release EVs at a more consistent rate, whereas there were many significant increases and decreases in particle release from SF (see figure 7), although this may be confounded by a possible contamination. The contaminating particles may have either a differing release pattern (if the contamination happened during hydrogel formation), or proliferation pattern.

Interesting to note is that, even with a possible contamination, the number of particles released for most EV groups from our samples derived from SF is substantially lower than that of our GelMA EV release studies. This is true for most groups except when comparing the highest concentrations of both groups, which both yielded an end cumulative release of around 60%, and an exceptionally large difference can be seen when comparing the cumulative release of lowest concentrations (where GelMA release was around 70% and SF release was around 30%). Although our results are not completely reliable due to the odd particle release from our blank SF groups, it thus seems likely that SF hydrogels would be better suited to reducing the burst release of EVs than

GelMA hydrogels, and a low concentration of SF without mesh would be expected to result in the longest EV release window. Extrapolating from our data, assuming that all particles counted in the release study of EV laden SF_3% without meshes were actually EVs, that no EVs were lost, and assuming that release remains similar to the first 14 days, it would take around 51 days for SF_3% to reach a release of 100%, far more than our initial goal of 14 days. The actual number of days it would take to reach 100% release would of course be expected to be lower, but the results remain promising.

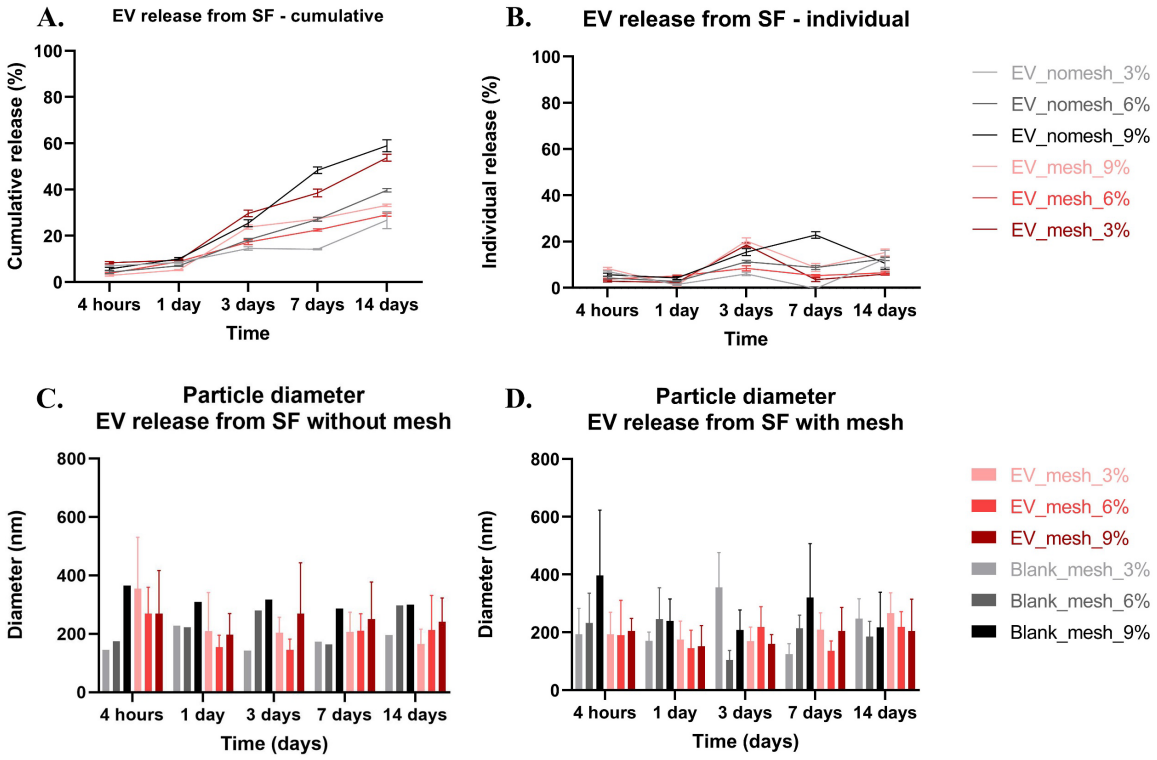


***Figure 6.*** *These graphs show EV release patterns from SF hydrogels, either cumulative release over time (A) or individual release per time point observed (B). Data was derived through nanoparticle tracking analysis. In addition, mean and standard error of particle diameters observed through NTA can be seen in graphs C (for hydrogels without meshes) and D (for hydrogels with meshes). In graphs C and D, particle diameters can be compared between hydrogel samples with (red) and without (black) EVs. No significant differences were found. For particle release graphs of control samples without EVs (blanks), see supplementary figure 1.*

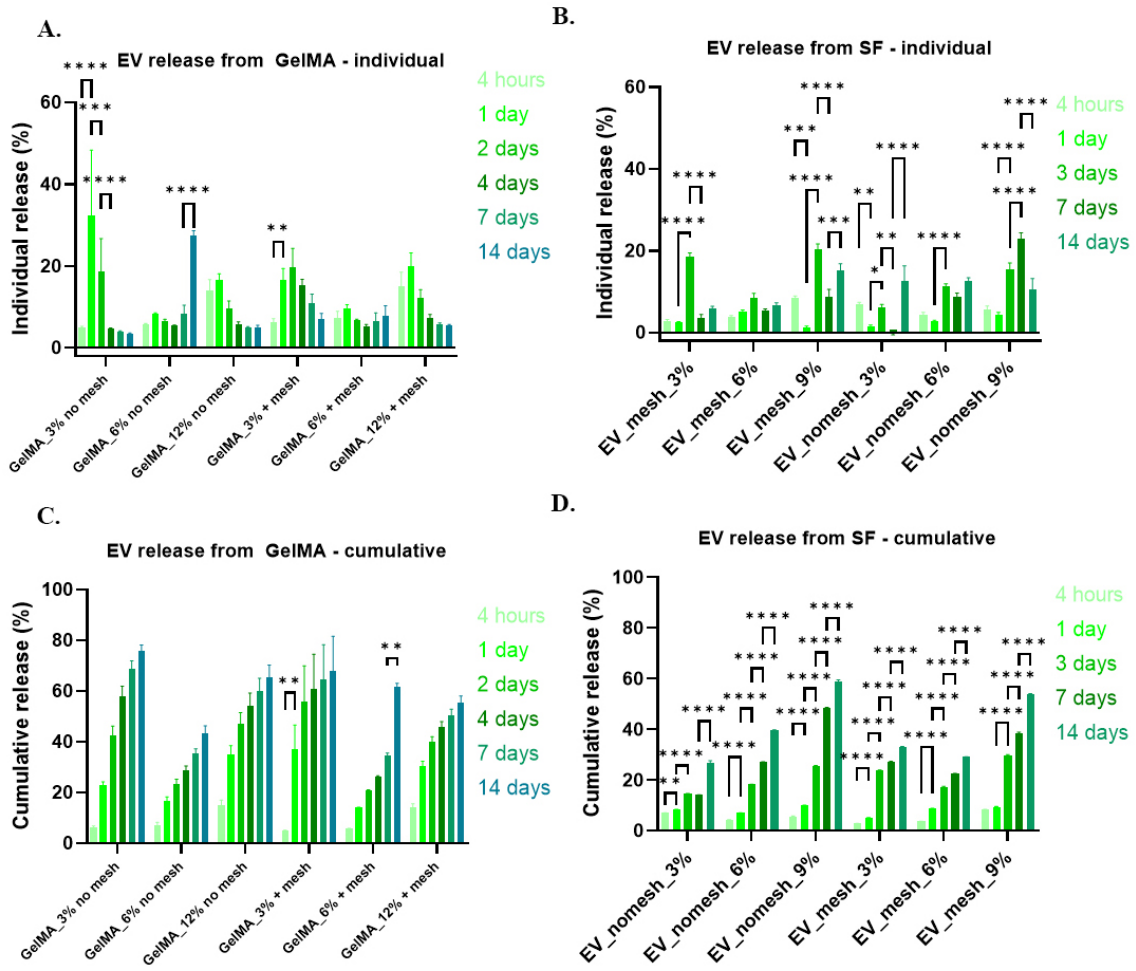


***Figure 7.*** *This bar graphs shows the release of EVs from GelMA and SF per group per time point based on individual release per time point (A and B), and cumulative data (C and D). Please note that significance has only been noted in the form of asterisks between time points that directly follow each other in order to keep the graphs somewhat legible.*

*3.3.4 Dynamic EV release*

As can be seen in figure 8, statistically significant differences were found between dynamic control groups without EVs and their respective concentration's groups with EVs for at least one comparison for all concentrations of SF analysed, indicating that a significant amount of EVs were indeed released from our hydrogel samples. For a full breakdown of all significant comparisons found via ordinary two-way ANOVA, please consult supplementary table 4. No significant differences were found in particle diameters between groups with and without extracellular vesicles. This is in line with the results with regards to particle diameter differences found in section 3.3.3. Concerning the difference in release between samples containing meshes or not, under static circumstances there seemed to be a small decrease in EV release as a result of mesh addition depending on SF concentration, where larger concentrations of gel enjoyed a larger decrease proportionally, although these differences were not deemed to be statistically significant according to an ordinary two-way ANOVA. The presence or absence of a mesh also didn't yield a significantly different result in particle release for groups subjected to dynamic loading, where only 2/6 groups show an increase in particle release for groups with a mesh as compared to their respective concentration under dynamic

loading without meshes. This is in line with our findings from the GelMA EV release tests described in 3.3.1 and most of our findings from the SF EV release tests described in 3.3.3, where the presence/absence of a mesh in the sample was found to have little to no effect on EV release.

As for differences in EV-release as a result of dynamic loading of the hydrogel samples, significant increases in particles released were only found between static and dynamic groups of the middle concentration of SF (6%), for both gels with and without meshes. In fact, SF_6% with meshes that were subjected to dynamic loading resulted in a highly significant ($p < 0.0001$) increase in EV-release as compared to gels with meshes subjected to dynamic loading of either lower or higher concentrations of SF. That this group performs worse in regard to delaying burst-release is unexpected from the results of our other tests, since SF_6% with mesh doesn't exhibit either significantly higher degradation, nor a significantly higher stiffness than other concentrations of SF with meshes from our degradation and amplitude sweep tests.

It is promising that there seems to be no significant difference in EV release depending on dynamic loading for both the higher and lower concentrations of SF, either with or without mesh, as this would mean that the dynamic environment of the heart would be unlikely to significantly affect the release of EVs from an end product made with SF of those concentrations, and further testing can be done on the release of EVs in light of that fact without having to take into account dynamic loading. This is good news, as dynamic loading, at least within the confines of the RMCU and the labs at the TU/e, is not possible to do within a completely sterile environment, as they do not have any universal testing machine, rheometer, or other machine capable of dynamic loading which can be placed and operated under a flow hood. Results from these dynamic release tests must then also be viewed critically with that fact in mind, that some variation may have crept into our data due to possible contamination. Although there were no significant differences observed in particle size, the aforementioned may have happened for example, with one or more samples of SF_6% dynamic with EVs and mesh. Even so, removing the highest concentration sample from that group's data set does nothing to reduce significance of the increase in EV-release between that group and groups within the same concentration, or samples under dynamic loading containing both EVs and meshes but with different concentrations.

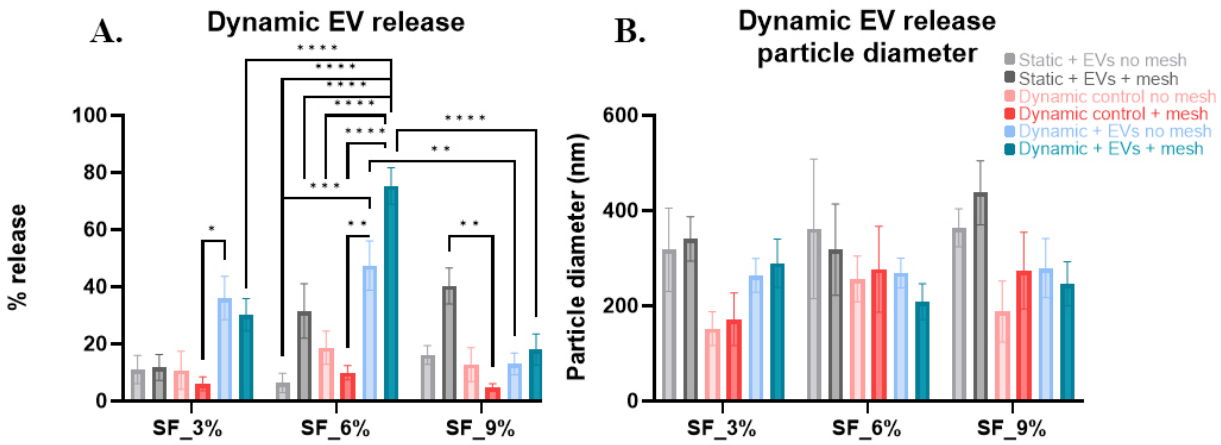


***Figure 8. A.*** *Bar plot showing EV-release % for dynamic release tests, bars in grey are static controls, while coloured bars denote results from samples subjected to dynamic loading (reds are controls without EVs while blues denote samples with EVs). Note that EV-release % is calculated based on EV-load of samples containing EVs even for those groups not containing EVs. Significance is shown between groups within the same concentration as well as between identical groups apart from concentration (e.g., two groups that both contain EVs and meshes and were subjected to dynamic loading, but do not have the same concentration). For a full breakdown of significant groups, see supplementary table 4.* ***B.*** *Bar plot showing mean and error for particle diameter for particles observed during dynamic release tests. Groups are the same as for A. No significant differences were found in particle diameter between groups.*

### 3.4 Mechanical and rheological testing

*3.4.1 Compression test*

Unfortunately, very few of the groups compared showed any significance (only GelMA_3% vs GelMA_12% without mesh, and SF_6% with mesh vs SF_6% without mesh). This is likely due to the high standard deviation we found (shown in supplementary figure 2 along with mean values per gel type), which in turn is likely due to the variation in values we can observe between replicates (shown in supplementary table 5). It is unclear what may be the reason for this high variation between replicates, although it may be due in part to differences in hydrogel temperature. Gel samples were cast on day 0 and transported to the lab in Eindhoven, where they were stored in the fridge. Then, at the start of day 1, gels were removed from the fridge and kept near the Criterion UTM for testing. This means that over time, gel temperature should have steadily increased to room temperature from 4 ºC. On each testing day, testing was begun with the lowest concentration of hydrogel, for which all replicates were then generated before moving on to the second-lowest concentration of hydrogel. As temperature differences between hydrogel samples should then be observed most between the samples tested at the start of the day (before room temperature had been reached), the highest variation between replicates, and therefore the highest standard deviation for the corresponding gel's Young's modulus, should then be observed in low-concentration gels. From viewing the standard deviations of our Young's moduli in figure 10, however, we can see that there is no such trend. It then remains unclear what caused the variation between replicates.

Although the differences between our groups are in general not significant (the only significant differences were found between GelMA_nomesh_3% vs. GelMA_nomesh_12% and between SF_nomesh_6% vs. SF_mesh_6%), we can see that mean Young's modulus for GelMA seems to increase with increased gel precursor concentration, and we can see a higher mean Young's modulus for each gel type when a mesh is added, where gels with higher concentrations of polymer seem to have a smaller increase in Young's modulus when a mesh is added as opposed to gels with low concentrations of polymer. This is in line with our expectations, as the addition of a mesh to our hydrogel should bring the Young's modulus of a gel closer to that of the mesh itself. In addition, increasing hydrogel concentration is expected to increase Young's modulus as well as increased polymer crosslinking density should logically increase stiffness of the construct.

Differences in yield strength seem to be negligible for most groups. Although the yield strength for both GelMA_12% groups seem to be a lot higher than for other groups, this is accompanied by an increase in standard deviation, so no conclusions can be reliably drawn from this data except that all our gels seem to have low deformation resistance. This makes sense as hydrogels consist mostly of water, which is purely viscous.

In addition to low deformation resistance our gels seem to show high ductility. Ductility seems higher for SF based gels as compared to GelMA gels, as GelMA gels show fracturing at higher strains, whereas the stress-strain curves of SF gels tell us that they experience more gradual failure with increased strain.

Even though the standard deviations of our results is high, the values we found for the Young's moduli of GelMA without meshes is in line with literature. For example, in the study done by Wu et al. (2019), who studied photo crosslinked GelMA with concentrations ranging from 5% to 30%, found Young's moduli that ranged from 3.08 kPa for 5% GelMA to 184.52 kPa for 30% GelMA. This study also found that, with increased stiffness of hydrogel constructs, the adhesion rate, viability, and spreading of cells is decreased, with 10% GelMA hydrogels being optimal for supporting the regeneration of PC12 cells. Whether this concentration would also be the ideal concentration for our purposes is unclear, as there is a significant difference between the Young's moduli of PC12 cells and cardiomyocytes, whereas PC12 cells have been found to have an average Young's modulus of 0.425 ± 0.03 kPa, the stiffness of cardiomyocytes is much higher even for a healthy heart with an average Young's modulus of around 18 kPa which can be increased to 2.5 MPa for pathological tissue (Allijn et al., 2020; Gopal et al., 2008).

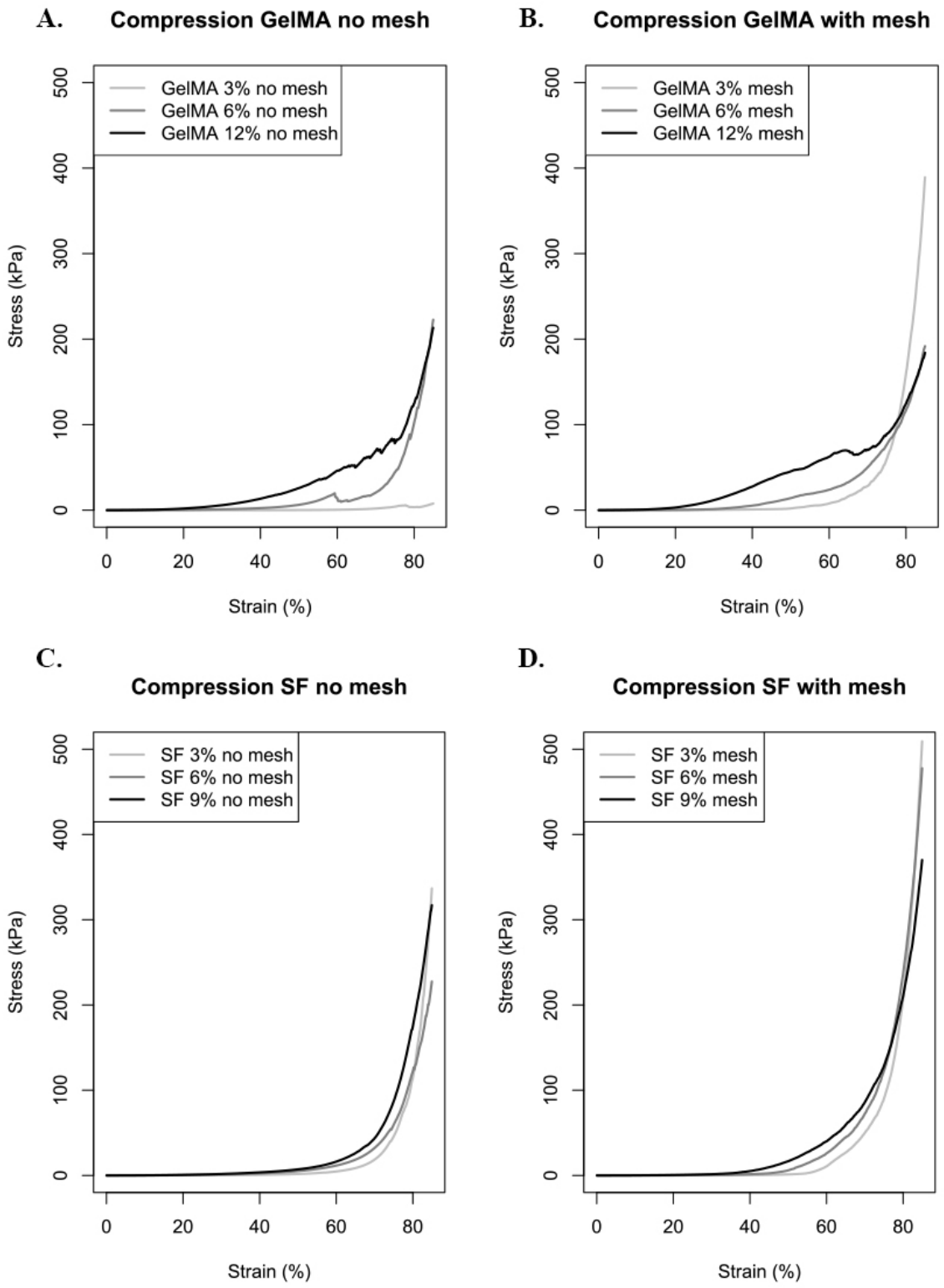


***Figure 9.*** *Stress-strain curves showing results of the compression tests for each gel-type with and without meshes. Note that these graphs show averages of each replicate, for more detailed graphs, see supplementary figure 2.*

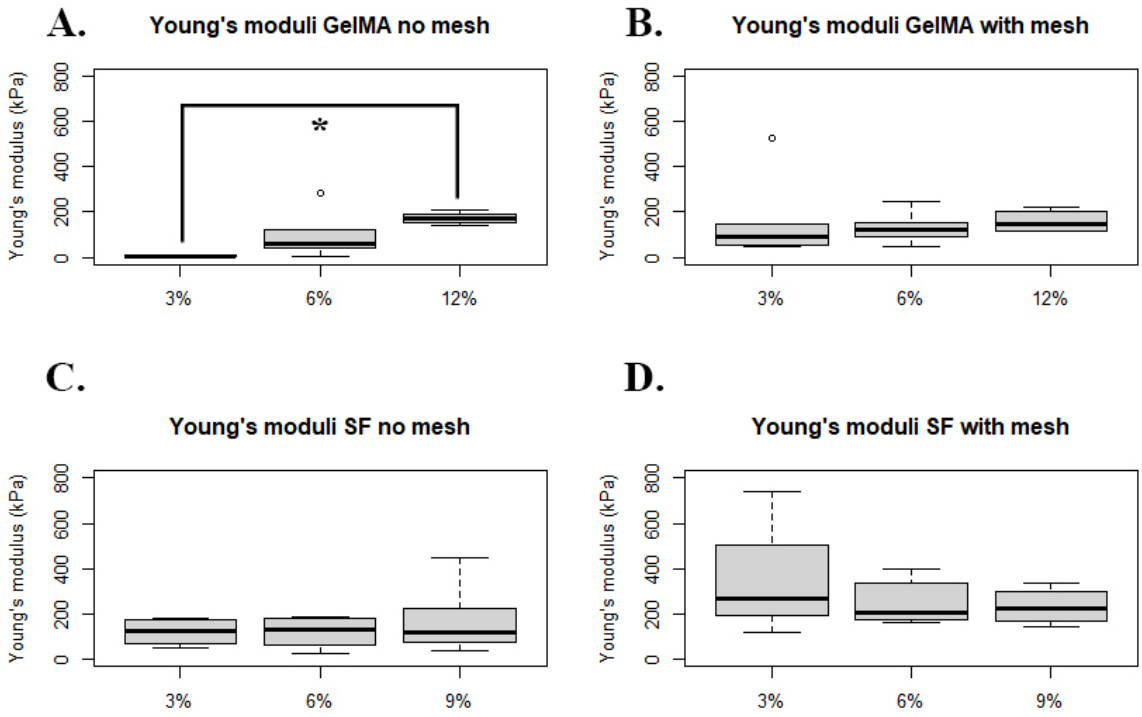


***Figure 10.*** *Boxplots showing five-number summaries of young's moduli for each gel type with and without meshes, calculated from results of compression tests. The only significant difference found (through T-testing) was found between GelMA_3% and GelMA_12% without meshes.*

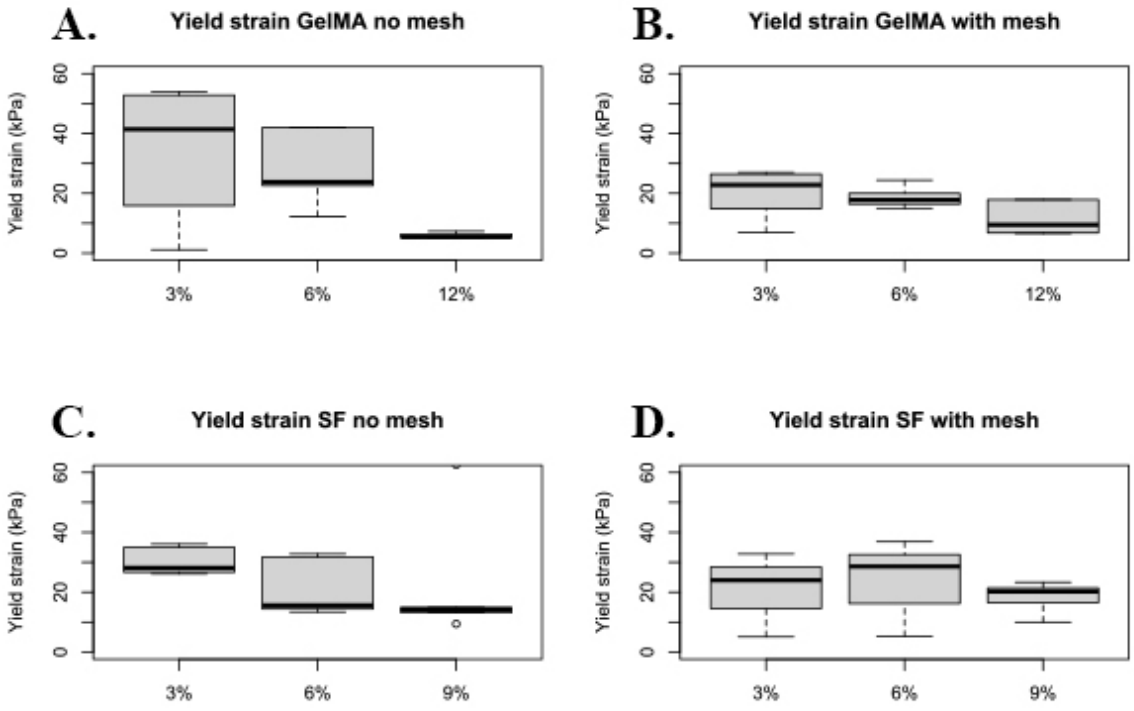


***Figure 11.*** *Boxplots showing the five-number summaries of yield strains per gel type with and without mesh. Derived from compression tests. No significant differences were found.*

*3.4.2 Stress-relaxation test*

According to research done by Chaudhuri et al. (2016), a decrease in relaxation period (defined as the time it takes for stress to decrease from the starting value by half and denoted as $\tau_{1/2}$) causes an increase in both cell proliferation and spreading. This is likely due to the increase in permeability that a decrease in relaxation period denotes. On the other hand, an extended $\tau_{1/2}$ of above 1 hour was found to suppress cell proliferation and spreading, which would be considered unacceptable for our product. In addition, stress relaxing hydrogels have been found to more readily release EVs (Lenzini et al., 2020). As can be seen in figure 12, none of our gels reached a $\tau_{1/2}$ that would be expected to suppress cell proliferation and spreading. A logarithmic scale was selected in visualising these graphs, as most relaxation occurs within the first minute or two for all groups. Visualising the data on a non-logarithmic scale results in graphs where the relaxation behaviour is difficult to compare. Examples of this have been shown with a representative sample (non-averaged data) in supplementary figure 5.

Through performing t-tests it was found that for SF, increasing the gel precursor concentration significantly decreases the relaxation period $\tau_{1/2}$ for samples without meshes while increasing the relaxation period for SF samples with a mesh. Some differences may have been obscured due to the high variance, especially in the case of GelMA_6% without meshes (see figure 12). Significant differences in $\tau_{1/2}$ for GelMA were only found between GelMA_3% and GelMA_12% without meshes, and between GelMA_12% with and without meshes. In each case of significance, the addition of a mesh increased the relaxation period. This is expected, as the addition of a mesh is expected to reduce elasticity and increase rigidity. This increased relaxation period indicates a lower permeability of the construct, and we therefore expected groups with a longer relaxation period to show a more prolonged EV release window. This seems to be the case in lower concentrations of GelMA when we take into account the results of the GelMA EV release tests, as the lowest concentration of GelMA correlates with a very high EV release. The release window seems to have less of an effect on SF hydrogels, although our results from their EV release tests remain muddled. From the results of these stress-relaxation tests, we may infer that the permeability and related EV release windows and cell spreading qualities of our construct may be tuned by careful selection of gel precursor concentration as well as addition of a PCL mesh. Our results also indicate that the impact of either permeability-tuning method differs according to hydrogel-type. For SF-based hydrogels, the presence of a mesh has a greater effect than adjusting gel prepolymer concentration, whereas the opposite seems true for GelMA hydrogels. It may be that this is because the relaxation behaviour of GelMA by itself is already similar to that of the PCL mesh, whereas SF exhibits quite a different relaxation pattern, and that adding a mesh to GelMA thus doesn't change that pattern very much, while changes caused by adjusting its concentration are more obvious. In other words, the effect of adding a mesh may be just as grand in pulling the relaxation behaviour towards a certain pattern in both gels, but because the relaxation behaviour of GelMA is already more similar to that of the PCL mesh, the effect seems lesser than in SF hydrogels.

As an aside, as we can see in figure 12 that stress at 15% strain is lower for higher gel concentrations at the beginning of each stress-relaxation test for all groups, indicating a higher stiffness. This is expected and in line with the results from compression tests and amplitude sweeps, which both suggest that higher concentrations of gel result in a stiffer hydrogel. In addition, as in the other tests indicating structure stiffness, we can see that the addition of a mesh increases stiffness most for low concentration GelMA, while the effect of the addition of a mesh on SF seems to be less pronounced.

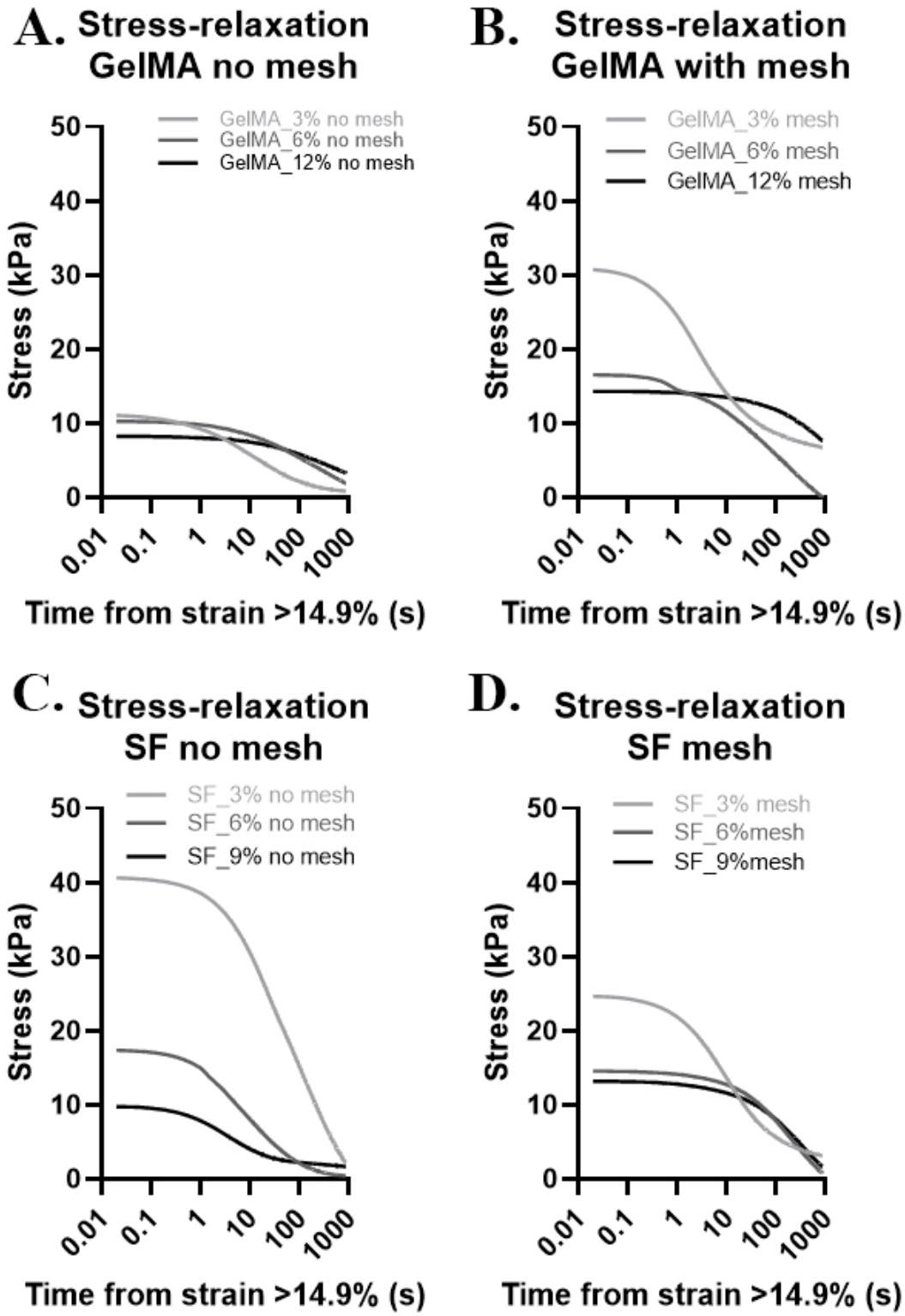


***Figure 12. A.&B.*** *Averaged stress-relaxation curves of GelMA + LAP hydrogel samples.* ***C.&D.*** *Averaged stress-relaxation curves of SF + Rb/SPS hydrogel samples. For all groups, strain was kept constant at 15%. Increasing gel concentration clearly increases relaxation time for all groups except SF without meshes. For more detailed plots per replication, view supplementary figure 4.*

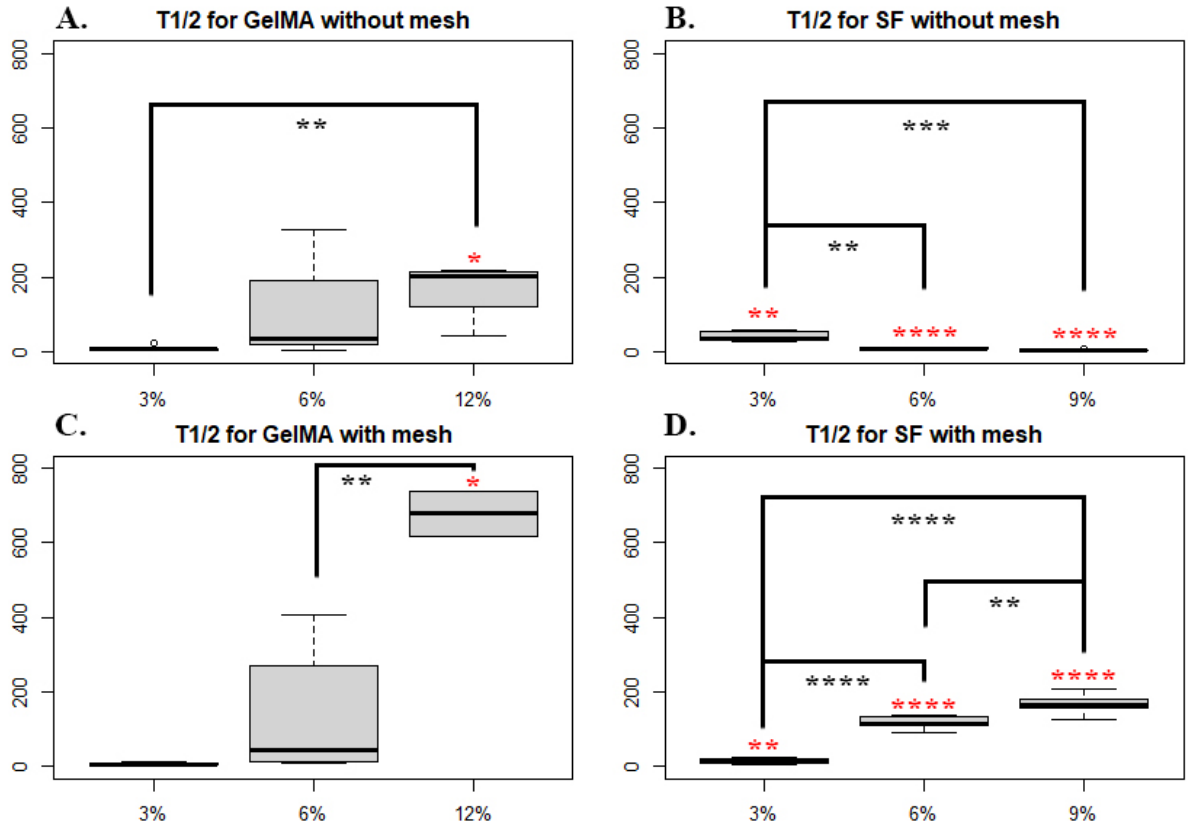


***Figure 13.*** *Boxplots showing the five-number summaries of τ1/2 in seconds per gel-type calculated from results of the unconfined stress-release tests done on gel samples without EVs submerged in PBS. Significant differences in τ1/2 were found between lowest and highest concentrations for each gel-type, between SF_3% and SF_6% without meshes, between GelMA_6% and GelMA_12%, and between all concentrations of SF with meshes. The addition of a mesh was found to significantly increase τ1/2 for GelMA_12% and for all concentrations of SF. Black asterisks are used to denote significance between gel concentrations, while red asterisks are used to denote the significance of the absence/presence of the MEW mesh for that gel-type and concentration.*

*3.4.3 Amplitude sweep*

For all gels, storage modulus (G') in the linear viscoelastic region (LVER) was higher than the loss modulus, indicating that our structures may be labelled as viscoelastic solids, and they behave as gel-like structures, which is expected. The LVER can be used as a measure of stability of the construct, where stability is dependent on LVER length (Rahali et al., 2017). Differences in LVER length can be observed between all groups, where in general longer LVERs can be observed in higher gel concentrations, gels without meshes, and SF gels vs GelMA (see figure 14). This indicates that SF gels are in general more stable than GelMA, which holds with the results of both the compression and degradation kinetics tests. LVER is difficult to ascertain in low concentration GelMA without mesh, which makes sense as these samples were extremely soft and often difficult to handle without breaking.

A decrease in G' indicates the start of decomposition of the internal structure of the construct, where a sharp downturn in the graph indicates a more brittle construct. Apart from the lowest concentration of GelMA (and less so for the lowest concentration of SF) without meshes, all our groups show this sharp downturn upon reaching their yield point, especially so for SF based gels. This means that our gels show a more brittle behaviour as a response to shear and indicates that they tend to break into multiple larger pieces rather than showing homogenous breakage. This is also expected, as homogenous breakage would be typical of i.e., a liquid or cream. Inhomogeneous breakage makes sense for hydrogels, as strain is increased beyond the yield strength, microfractures start to appear in the construct as crosslinks are broken. As these microfractures develop, energy is lost, and we see a gradual increase in the loss modulus (G"). As long as G'>G", the structure is held together somewhat in one piece, but as the strain increases a microfracture develops, the structure ruptures, and we can see a crossover point in the moduli (G'=G") as the structure enters a flowing state.

In addition, the height of G' in the LVER can be used as a measure of strength/stiffness. In our results, we can see that an increase in gel concentration for gels without meshes produces a significant increase in gel strength. Increasing gel concentration beyond 6% in SF doesn't seem to produce a significant further increase in gel strength, however. The addition of a mesh seems to significantly increase construct strength for both GelMA and SF hydrogels, with a greater effect for low gel concentrations. This is in line with the conclusions suggested from our compression test results.

The crossover point strain is significantly decreased for gels without meshes at higher gel concentrations for both gel-types (where crossover occurs at significantly greater strains for SF gels vs GelMA). This may be due to the increased stiffness that comes with the increase in crosslinks for higher gel percentages. Structures containing meshes also showed a significant decrease in the crossover point strain, likely due to the added stiffness provided by the mesh. Interestingly, low concentration gels seem to be more affected by the addition of a mesh in this regard than high concentration gels, although the crossover point was lower for each group with mesh compared to its corresponding gel type and concentration without mesh.

When comparing our results of the amplitude sweep test with those of the compression test, it seems as though the effect of the addition of a mesh is much higher in the amplitude sweep tests. It seems likely that this is due to the manner in which strain is applied to the hydrogel sample in relation to the mesh. In the compression test, compression is applied in a vertical manner, perpendicular to the mesh. On the other hand, in this amplitude sweep, samples are strained through rotation of the upper contact point with the rheometer, thus creating shear stress that is parallel with the mesh. Because of this, it is likely that the mesh itself has stiffer properties in the horizontal axis than in the vertical axis, and thus has a larger effect on our outcomes when being strained horizontally, especially for low concentration hydrogels.

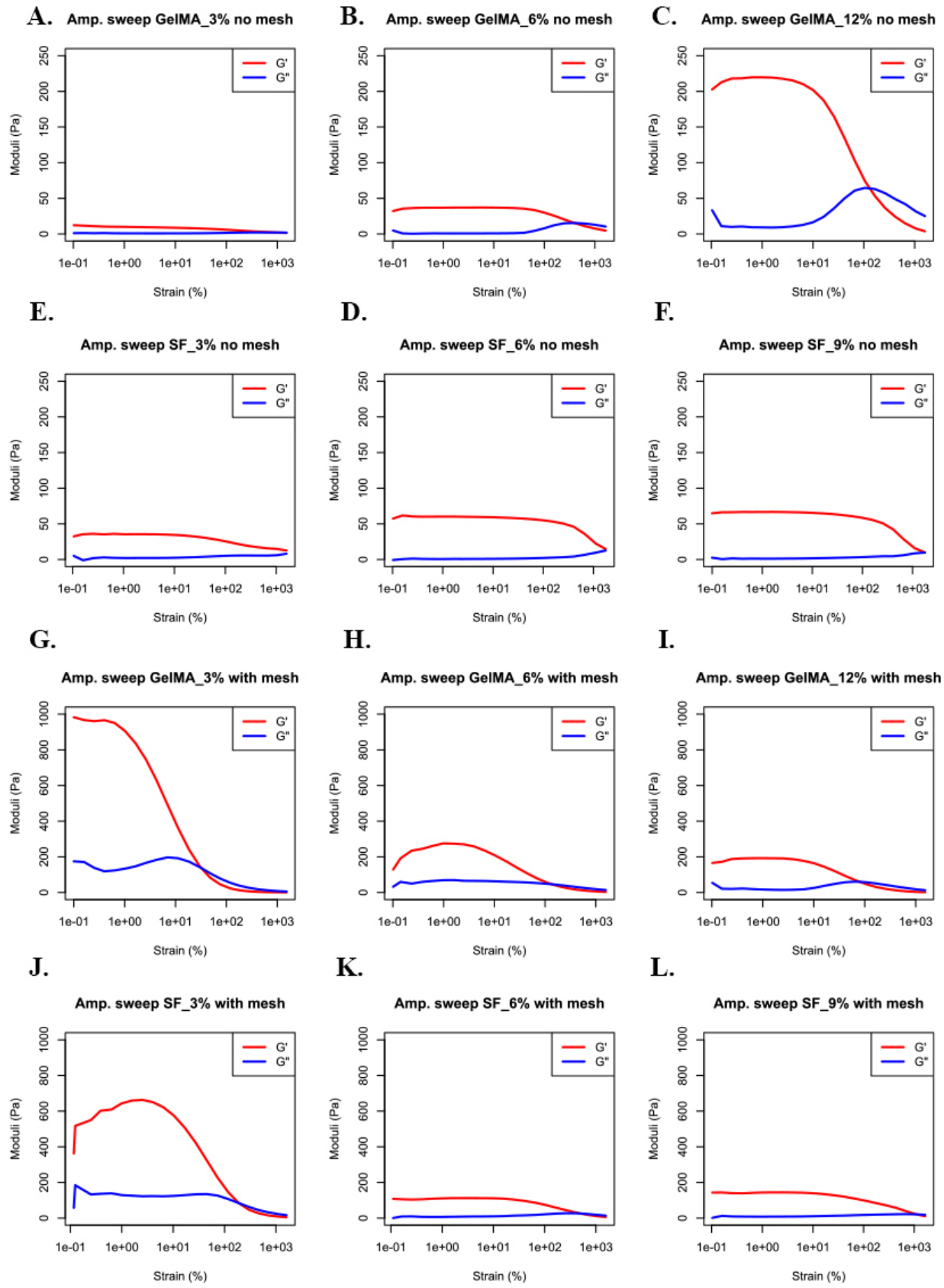


***Figure 14.*** *Shows storage and loss moduli depending on strain, for each gel type. This data was gathered through amplitude sweeps. For more detailed graphs, see supplementary figure 6. Note that the scale of the y-axis differs for gels with and without meshes, as otherwise these graphs would be unreadable.*

*3.4.4 Frequency sweep*

From results from compression testing and amplitude sweeps, it was determined that 1% strain would be appropriate for the conductance of the frequency sweeps, as this value seems to be within the LVER for all groups (Rahali et al., 2017). As we can see from the results of the frequency sweeps in figure 15, the storage modulus is higher than the loss modulus for all groups throughout the test, indicating the solid nature of the structures. It seems as though these values are not particularly dependent on frequency, as the values for both G' and G" stay relatively constant with increased frequency. A striking exception to this is GelMA_3% without meshes, which shows a small decrease followed by a steady increase in G'. This observation may be due to the very small value of G' for GelMA_3% when compared to other groups, most of which have storage moduli which hover around a couple hundred Pa. A larger proportion of the values and differences over time/frequencies for G' is therefore due to noise, and it is difficult to draw conclusions for it.

For all groups except GelMA without meshes, there seems to be a very slight decrease in G' at high frequencies for the highest concentrations. These decreases are accompanied by minute increases in G", which indicates that due to the brittle nature of these higher concentrations of gels may cause the appearance of microfractures in the structure at high frequencies. This indicates that these high-concentration gels may not be as stable as lower concentration gels over long periods of time where the structures are subjected to movements such as those that our structures may experience in the dynamic cardiac environment.

Additionally, the absence of any crossover points between G' and G" indicates that our gels feature a tangled fibrous network and is thus non-reversibly crosslinked (Stojkov et al., 2021). In addition, the storage modulus was always higher than the loss modulus, indicating that the hydrogel have a solid-like structure due to physical crosslinking. As with the amplitude sweep, the height of the G' plateaus is a measure of stiffness of the construct, and we can see that our assessments of the different groups' stiffnesses from the previous amplitude sweep are corroborated by the results of this test. Once again, we can see that stiffness is dependent on gel type, concentration, and mesh presence, and could conceivably be tuned by adjusting these.

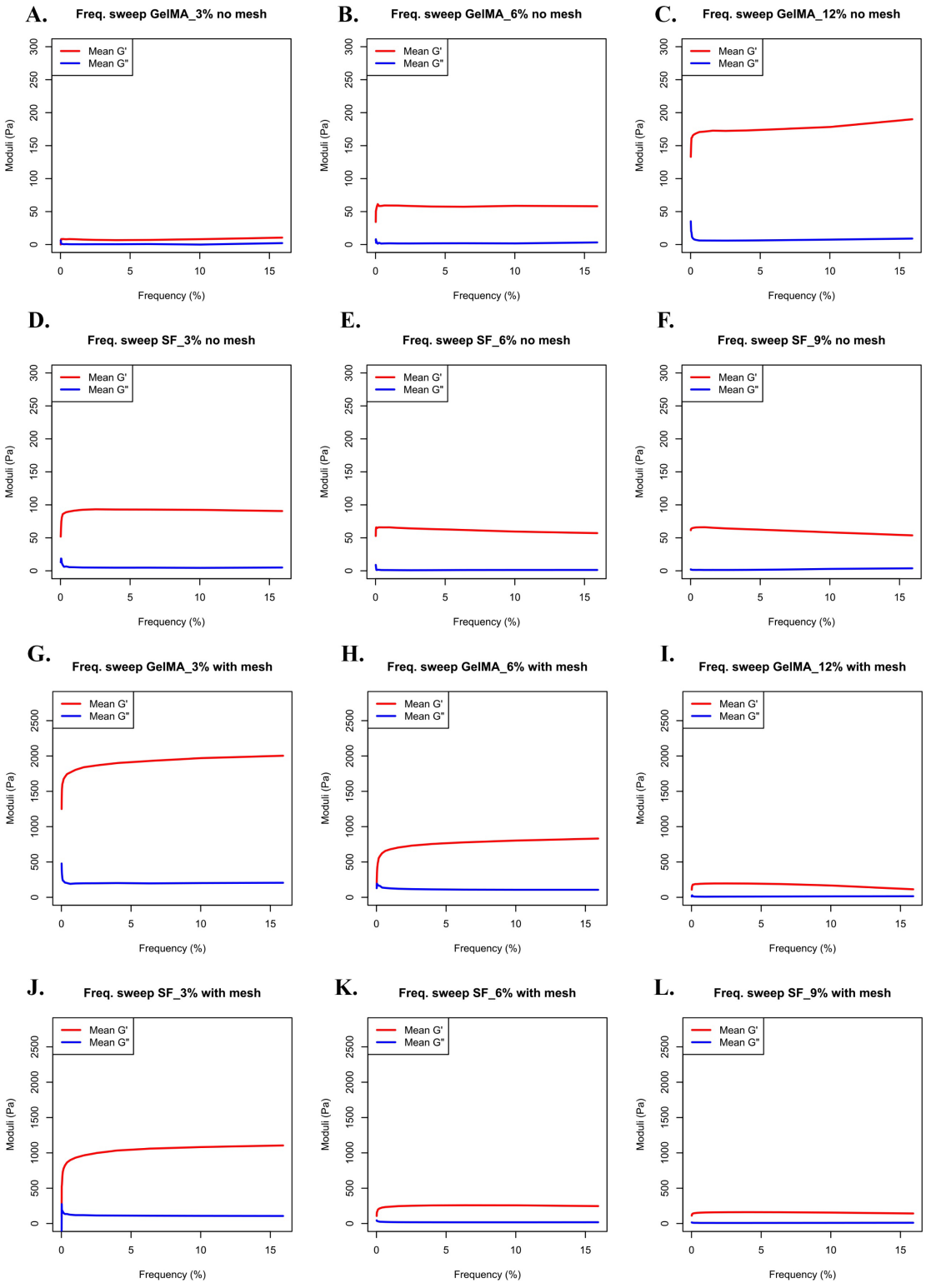


***Figure 15.*** *Curve showing frequency dependence for storage and loss moduli of all different conditions (gel type, concentration, mesh/no mesh). Curves show averaged data from replicates, for graphs showing individual curves per replicate, please view supplementary figure 7. Please note that y-axis scales differ between groups with and without meshes in order to maintain legibility.*

## 4. Conclusions

Our research question pertained to the feasibility of EV release tuning. From our results, it seems clear that the EV release window from hydrogels can be tuned by adjusting the mechanical and degradation properties of the hydrogel. Our expectations were that use of silk-based hydrogels at lower concentrations without a MEW mesh would result in the longest EV release window, while GelMA hydrogels at higher concentrations with a MEW mesh, especially within a dynamic environment, would feature a reduced EV release window. In light of the results discussed, our hypotheses that EV release patterns are dependent on hydrogel selection, concentration, MEW mesh presence, and dynamic loading all hold. Factors which had a particularly large impact on EV release were hydrogel degradation, construct stiffness, and a dynamic environment. Low and high (3% and 12%) concentrations of GelMA seem not to be ideal for the delay of EV release, and GelMA hydrogels in general seem to cause significant burst release of EVs around day 1-2 of incubation. For GelMA, the addition of a mesh caused no significant differences in EV release overall. When selecting GelMA, 6% seems to perform best in delaying EV release, likely due to the balance between degradation patterns and stiffness that this concentration of GelMA displays. Although there were significant issues with the measurements of EV release from SF, it seems likely that EV release from SF is slower than in GelMA, as peak EV release is delayed by 1-5 days and particle release was found to be lower in general. For SF, there seems to be a very weak relationship between EV release and mesh presence, where the addition of a mesh resulted in slightly fewer particles being release, though not significant. For SF it is difficult to ascertain which concentration would be ideal for delaying EV release. SF_3% performed best within the EV release tests proper, however, this test had significant issues (likely due to contamination and repeated freeze-thaw cycles) and results from this test are thus not completely trustworthy. When regarding the dynamic release test of EVs from SF, it would conversely appear that high concentrations of SF perform best with regards to delaying EV release. Regardless, silk fibroin hydrogels seem to be the superior choice both in terms of stability and mechanical properties, even at low concentrations. An extremely important factor in terms of EV release, especially with regards to the envisioned cardioprotective purposes of the proposed constructs, is the (dynamic) environment within which the hydrogel constructs reside. Dynamic loading of the hydrogel clearly causes an increase in EV release, although this effect is much smaller for high concentrations of SF.

## 5. Future research

In future research, EV release tests should be done on silk fibroin hydrogels to confirm the suggestion from our research that these hydrogels have lower and slower EV release patterns. It would be especially interesting to study the effects of dynamic loading on EV release from these hydrogels more long-term and within an environment that resembles the cardiac environment better. This could be especially important to investigate in order to select the ideal concentration of silk-based hydrogel, as in our frequency sweep test it was found that higher concentrations of hydrogel are more brittle and may exhibit microfractures when exposed to dynamic loading over a longer period of time. Although within our dynamic loading test we found the highest concentration of SF to release the lowest percentage of EV release, it would be interesting to see if this pattern persists when the hydrogel is subject to dynamic loading for a longer period to investigate whether these microfractures have an unwanted effect on EV release.

From our research, the effects of mesh presence have seemed minimal, and this may be due to their small volume in proportion to the volume of hydrogel used. As such, it might be interesting for future researchers to investigate the effects of the addition of a larger MEW mesh on mechanical and EV release properties.

In addition, the EV release properties of the hydrogels used could in theory be tuned further through adjusting the photoinitiator concentrations, as a preprint study done by Born et al. (2021) indicated that LAP concentrations of 0.1% w/v in mesenchymal stem cell-derived EV-laden GelMA resulted in a significant burst release of EVs from the construct, whereas higher concentrations of LAP resulted in a prolonged EV release window. EV release properties, and potentially cell viability, may also be tuned by the creation of an interpenetrating network. The creation of an interpenetrating

network containing both a SF-based hydrogel and GelMA may result in a hydrogel that is stronger and has a longer degradation period than GelMA provides on its own, without foregoing the biological cues that are provided by GelMA. Increasing GelMA may increase speed of degradation, as well as cell adhesion. An added advantage to mixing in GelMA with a SF based hydrogel is that the gelation period is significantly decreased. Overall, the creation of a hydrogel containing both GelMA and SilkMA would increase tunability for a wide array of mechanical and rheological characteristics, resulting in a construct that is better adapted to the successful delayed delivery of EVs (and possibly cardiomyocytes and cardiac fibroblasts) to cardiac tissue than a single component hydrogel would be.

Although EV uptake studies and HUVEC tube formation assays were outside the scope of this research, these studies could give important information on the effectiveness of the proposed constructs support and promotion of angiogenesis and cardiomyocyte proliferation, as well as shedding more light on the therapeutic window of EVs. For this purpose, the constructs could be further loaded with cardiomyocytes and cardiac fibroblasts. Based on results from these tests, hydrogel properties could be tuned further using the information gathered in this research.

In future, the best application method for this construct to the heart could also be investigated. One feasible method in which to apply a cardiac patch to the heart may be through a catheter-like tube followed by affixation through the application of fibrin glue around the edges of the construct. This method has been shown to be suitable for the application of cardiac patches, showing no major complications in tests on porcine model organisms, and having the added benefit of removing the need for open-heart surgery (Montgomery et al., 2017). This method is suitable for a construct that is on the softer and weaker side, such as is the case with most hydrogels. A stronger and more resilient construct on the other hand, could feasibly be sutured to the cardiac surface. For our gels, their mechanical strength is thus that application with fibrin glue is the more realistic option.

Lastly, the avenue of extrusion printing of the hydrogel portion of our constructs would be interesting to be investigated, especially if the avenue of MEW mesh insertion into the hydrogel construct is to be followed, as the RegenHU printer through which the MEW meshes were created would allow for the production of the construct to be done solely via the RegenHU printer, and this streamlined process could save time, logistics, and money, while enabling the creation of custom shapes for the construct without necessitating creation of specific Teflon moulds.

## 6. References:


Allevi Support. (2020, June 23). *Gelatin Methacrylate (GelMA) Guide*. https://www.allevi3d.com/gelatin-methacrylate-guide/

Allijn, I., Ribeiro, M., Poot, A., Passier, R., & Stamatialis, D. (2020). Membranes for modelling cardiac tissue stiffness in vitro based on poly(Trimethylene carbonate) and poly(ethylene glycol) polymers. *Membranes*, *10*(10), 1–12. https://doi.org/10.3390/membranes10100274

Arslan, F., Lai, R. C., Smeets, M. B., Akeroyd, L., Choo, A., Aguor, E. N. E., Timmers, L., van Rijen, H. v., Doevendans, P. A., Pasterkamp, G., Lim, S. K., & de Kleijn, D. P. (2013). Mesenchymal stem cell-derived exosomes increase ATP levels, decrease oxidative stress and activate PI3K/Akt pathway to enhance myocardial viability and prevent adverse remodeling after myocardial ischemia/reperfusion injury. *Stem Cell Research*, *10*(3), 301–312. https://doi.org/10.1016/j.scr.2013.01.002

Assmus, B., Schächinger, V., Teupe, C., Britten, M., Lehmann, R., Döbert, N., Grünwald, F., Aicher, A., Urbich, C., Martin, H., Hoelzer, D., Dimmeler, S., & Zeiher, A. M. (2002). Transplantation of progenitor cells and regeneration enhancement in acute myocardial infarction (TOPCARE-AMI). *Circulation*, *106*(24), 3009–3017. https://doi.org/10.1161/01.CIR.0000043246.74879.CD

Barroso, I. A., Man, K., Villapun, V. M., Cox, S. C., & Ghag, A. K. (2021). Methacrylated Silk Fibroin Hydrogels: PH as a Tool to Control Functionality. *ACS Biomaterials Science and Engineering*, *7*(10), 4779–4791. https://doi.org/10.1021/acsbiomaterials.1c00791

Bejleri, D., Streeter, B. W., Nachlas, A. L. Y., Brown, M. E., Gaetani, R., Christman, K. L., & Davis, M. E. (2018). A Bioprinted Cardiac Patch Composed of Cardiac-Specific Extracellular Matrix and Progenitor Cells for Heart Repair. *Advanced Healthcare Materials*, *7*(23). https://doi.org/10.1002/adhm.201800672

Born, L. J., Mcloughlin, S. T., Dutta, D., Mahadik, B., Jia, X., Fisher, J. P., & Jay, S. M. (2021). Sustained Released of Bioactive Mesenchymal Stromal Cell-Derived Extracellular 1 Vesicles from 3D-Printed Gelatin Methacrylate Hydrogels 2. *BioRxiv*. https://doi.org/10.1101/2021.09.28.462252

Buikema, J. W., van der Meer, P., Sluijter, J. P. G., & Domian, I. J. (2013). Concise review: Engineering myocardial tissue: The convergence of stem cells biology and tissue engineering technology. *Stem Cells*, *31*(12), 2587–2598. https://doi.org/10.1002/stem.1467

Cambria, E., Pasqualini, F. S., Wolint, P., Günter, J., Steiger, J., Bopp, A., Hoerstrup, S. P., & Emmert, M. Y. (2017). Translational cardiac stem cell therapy: advancing from first-generation to next-generation cell types. *Npj Regenerative Medicine*, *2*(1). https://doi.org/10.1038/s41536-017-0024-1

Castilho, M., van Mil, A., Maher, M., Metz, C. H. G., Hochleitner, G., Groll, J., Doevendans, P. A., Ito, K., Sluijter, J. P. G., & Malda, J. (2018). Melt Electrowriting Allows Tailored Microstructural and Mechanical Design of Scaffolds to Advance Functional Human Myocardial Tissue Formation. *Advanced Functional Materials*, *28*(40). https://doi.org/10.1002/adfm.201803151

Central Bureau for Statistics. (2021). *Statistics Netherlands: Overledenen; belangrijke doodsorzaken (korte lijst), leeftijd, geslacht*. https://opendata.cbs.nl/statline/#/CBS/nl/dataset/7052_95/table?ts=1638965716930

Chaudhuri, O., Gu, L., Klumpers, D., Darnell, M., Bencherif, S. A., Weaver, J. C., Huebsch, N., Lee, H. P., Lippens, E., Duda, G. N., & Mooney, D. J. (2016). Hydrogels with

tunable stress relaxation regulate stem cell fate and activity. *Nature Materials*, *15*(3), 326–334. https://doi.org/10.1038/nmat4489

Cui, X., Li, J., Hartanto, Y., Durham, M., Tang, J., Zhang, H., Hooper, G., Lim, K., & Woodfield, T. (2020). Advances in Extrusion 3D Bioprinting: A Focus on Multicomponent Hydrogel-Based Bioinks. In *Advanced Healthcare Materials* (Vol. 9, Issue 15). Wiley-VCH Verlag. https://doi.org/10.1002/adhm.201901648

Das, S., Pati, F., Chameettachal, S., Pahwa, S., Ray, A. R., Dhara, S., & Ghosh, S. (2013). Enhanced redifferentiation of chondrocytes on microperiodic silk/gelatin scaffolds: Toward tailor-made tissue engineering. *Biomacromolecules*, *14*(2), 311–321. https://doi.org/10.1021/bm301193t

Davidson, S. M., Boulanger, C. M., Aikawa, E., Badimon, L., Barile, L., Binder, C. J., Brisson, A., Buzas, E., Emanueli, C., Jansen, F., Katsur, M., Lacroix, R., Lim, S. K., Mackman, N., Mayr, M., Menasché, P., Nieuwland, R., Sahoo, S., Takov, K., … Sluijter, J. P. G. (2022). Methods for the identification and characterization of extracellular vesicles in cardiovascular studies: from exosomes to microvesicles. *Cardiovascular Research*. https://doi.org/10.1093/cvr/cvac031

de Ruijter, M., Ribeiro, A., Dokter, I., Castilho, M., & Malda, J. (2019). Simultaneous Micropatterning of Fibrous Meshes and Bioinks for the Fabrication of Living Tissue Constructs. *Advanced Healthcare Materials*, *8*(7). https://doi.org/10.1002/adhm.201800418

Ding, H., Illsley, N. P., & Chang, R. C. (2019). 3D Bioprinted GelMA Based Models for the Study of Trophoblast Cell Invasion. *Scientific Reports*, *9*(1). https://doi.org/10.1038/s41598-019-55052-7

Doyle, L. M., & Wang, M. Z. (2019). Overview of extracellular vesicles, their origin, composition, purpose, and methods for exosome isolation and analysis. In *Cells* (Vol. 8, Issue 7). MDPI. https://doi.org/10.3390/cells8070727

Fine, B., & Vunjak-Novakovic, G. (2020). Heart regeneration in mouse and human: a bioengineering perspective. In *Current Opinion in Physiology* (Vol. 14, pp. 56–63). Elsevier Ltd. https://doi.org/10.1016/j.cophys.2020.01.004

Gaceb, A., Martinez, M. C., & Andriantsitohaina, R. (2014). Extracellular vesicles: New players in cardiovascular diseases. In *International Journal of Biochemistry and Cell Biology* (Vol. 50, Issue 1, pp. 24–28). Elsevier Ltd. https://doi.org/10.1016/j.biocel.2014.01.018

Gopal, A., Luo, Z., Lee, J. Y., Kumar, K., Li, B., Hoshino, K., Schmidt, C., Ho, P. S., & Zhang, X. (2008). Nano-opto-mechanical characterization of neuron membrane mechanics under cellular growth and differentiation. *Biomedical Microdevices*, *10*(5), 611–622. https://doi.org/10.1007/s10544-008-9172-9

Gu, L., Li, T., Song, X., Yang, X., Li, S., Chen, L., Liu, P., Gong, X., Chen, C., & Sun, L. (2021). Preparation and characterization of methacrylated gelatin/bacterial cellulose composite hydrogels for cartilage tissue engineering. *Regenerative Biomaterials*, *7*(2), 195–202. https://doi.org/10.1093/RB/RBZ050

Hafiane, A., & Daskalopoulou, S. S. (2018). Extracellular vesicles characteristics and emerging roles in atherosclerotic cardiovascular disease. In *Metabolism: Clinical and Experimental* (Vol. 85, pp. 213–222). W.B. Saunders. https://doi.org/10.1016/j.metabol.2018.04.008

Hromada, C., Mühleder, S., Grillari, J., Redl, H., & Holnthoner, W. (2017). Endothelial extracellular vesicles-promises and challenges. In *Frontiers in Physiology* (Vol. 8, Issue MAY). Frontiers Research Foundation. https://doi.org/10.3389/fphys.2017.00275

ICNIRP. (2004). *INTERNATIONAL COMMISSION ON NON-IONIZING RADIATION PROTECTION ICNIRP GUIDELINES ON LIMITS OF EXPOSURE TO*

*ULTRAVIOLET RADIATION OF WAVELENGTHS BETWEEN 180 nm AND 400 nm (INCOHERENT OPTICAL RADIATION) ICNIRP Guidelines GUIDELINES ON LIMITS OF EXPOSURE TO ULTRAVIOLET RADIATION OF WAVELENGTHS BETWEEN 180 NM AND 400 NM (INCOHERENT OPTICAL RADIATION) The International Commission on Non-Ionizing Radiation Protection**.

Kapoor, S., & Kundu, S. C. (2016). Silk protein-based hydrogels: Promising advanced materials for biomedical applications. In *Acta Biomaterialia* (Vol. 31, pp. 17–32). Elsevier Ltd. https://doi.org/10.1016/j.actbio.2015.11.034

Khan, F., Tanaka, M., & Ahmad, S. R. (2015). Fabrication of polymeric biomaterials: a strategy for tissue engineering and medical devices. In *Journal of Materials Chemistry B* (Vol. 3, Issue 42, pp. 8224–8249). Royal Society of Chemistry. https://doi.org/10.1039/c5tb01370d

Kim, E., Seok, J. M., Bae, S. bin, Park, S. A., & Park, W. H. (2021). Silk fibroin enhances cytocompatibilty and dimensional stability of alginate hydrogels for light-based three-dimensional bioprinting. *Biomacromolecules*, *22*(5), 1921–1931. https://doi.org/10.1021/acs.biomac.1c00034

Kim, H. H., Kim, J. W., Choi, J., Park, Y. H., & Ki, C. S. (2018). Characterization of silk hydrogel formed with hydrolyzed silk fibroin-methacrylate via photopolymerization. *Polymer*, *153*, 232–240. https://doi.org/10.1016/j.polymer.2018.08.019

Kim, S. H., Hong, H., Ajiteru, O., Sultan, Md. T., Lee, Y. J., Lee, J. S., Lee, O. J., Lee, H., Park, H. S., Choi, K. Y., Lee, J. S., Ju, H. W., Hong, I.-S., & Park, C. H. (2021). 3D bioprinted silk fibroin hydrogels for tissue engineering. *Nature Protocols*, *16*(12), 5484–5532. https://doi.org/10.1038/s41596-021-00622-1

Koti, P., Muselimyan, N., Mirdamadi, E., Asfour, H., & Sarvazyan, N. A. (2019). Use of GelMA for 3D printing of cardiac myocytes and fibroblasts. *Journal of 3D Printing in Medicine*, *3*(1), 11–22. https://doi.org/10.2217/3dp-2018-0017

Koudstaal, S., Jansen of Lorkeers, S. J., Gaetani, R., Gho, J. M. I. H., van Slochteren, F. J., Sluijter, J. P. G., Doevendans, P. A., Ellison, G. M., & Chamuleau, S. A. J. (2013). Concise Review: Heart Regeneration and the Role of Cardiac Stem Cells. *STEM CELLS Translational Medicine*, *2*(6), 434–443. https://doi.org/10.5966/sctm.2013-0001

Lee, C., Mitsialis, ; S Alex, Aslam, M., Vitali, S. H., Vergadi, E., Konstantinou, G., Sdrimas, K., Fernandez-Gonzalez, A., & Kourembanas, S. (2012). *Vascular Medicine Exosomes Mediate the Cytoprotective Action of Mesenchymal Stromal Cells on Hypoxia-Induced Pulmonary Hypertension*. https://doi.org/10.1161/CIRCULATIONAHA

Lenzini, S., Bargi, R., Chung, G., & Shin, J. W. (2020). Matrix mechanics and water permeation regulate extracellular vesicle transport. In *Nature Nanotechnology* (Vol. 15, Issue 3, pp. 217–223). Nature Research. https://doi.org/10.1038/s41565-020-0636-2

Li, Y., Liu, B., Chen, Y., Quan, X., Han, Y., Zheng, Y., & Zhao, Y. (2021). Extracellular Vesicle Application as a Novel Therapeutic Strategy for Ischemic Stroke. In *Translational Stroke Research*. Springer. https://doi.org/10.1007/s12975-021-00915-3

Lim, K. S., Klotz, B. J., Lindberg, G. C. J., Melchels, F. P. W., Hooper, G. J., Malda, J., Gawlitta, D., & Woodfield, T. B. F. (2019). Visible Light Cross-Linking of Gelatin Hydrogels Offers an Enhanced Cell Microenvironment with Improved Light Penetration Depth. *Macromolecular Bioscience*, *19*(6). https://doi.org/10.1002/mabi.201900098

Lim, K. S., Schon, B. S., Mekhileri, N. v., Brown, G. C. J., Chia, C. M., Prabakar, S., Hooper, G. J., & Woodfield, T. B. F. (2016). New Visible-Light Photoinitiating System for Improved Print Fidelity in Gelatin-Based Bioinks. *ACS Biomaterials Science and Engineering*, *2*(10), 1752–1762. https://doi.org/10.1021/acsbiomaterials.6b00149

Louro, A. F., Paiva, M. A., Oliveira, M. R., Kasper, K. A., Alves, P. M., Gomes-Alves, P., & Serra, M. (2022). Bioactivity and miRNome Profiling of Native Extracellular Vesicles in

Human Induced Pluripotent Stem Cell-Cardiomyocyte Differentiation. *Advanced Science*, *9*(15). https://doi.org/10.1002/advs.202104296

Maheshwari, R., Tekade, M., Gondaliya, P., Kalia, K., D'Emanuele, A., & Tekade, R. K. (2017). Recent advances in exosome-based nanovehicles as RNA interference therapeutic carriers. In *Nanomedicine* (Vol. 12, Issue 21, pp. 2653–2675). Future Medicine Ltd. https://doi.org/10.2217/nnm-2017-0210

Malda, J., Visser, J., Melchels, F. P., Jüngst, T., Hennink, W. E., Dhert, W. J. A., Groll, J., & Hutmacher, D. W. (2013). 25th anniversary article: Engineering hydrogels for biofabrication. In *Advanced Materials* (Vol. 25, Issue 36, pp. 5011–5028). https://doi.org/10.1002/adma.201302042

Markiewicz, M., Richard, E., Marks, N., & Ludwicka-Bradley, A. (2013). Impact of endothelial microparticles on coagulation, inflammation, and angiogenesis in age-related vascular diseases. In *Journal of Aging Research* (Vol. 2013). https://doi.org/10.1155/2013/734509

Meyer, G. P., Wollert, K. C., Lotz, J., Steffens, J., Lippolt, P., Fichtner, S., Hecker, H., Schaefer, A., Arseniev, L., Hertenstein, B., Ganser, A., & Drexler, H. (2006). Intracoronary bone marrow cell transfer after myocardial infarction: Eighteen months' follow-up data from the randomized, controlled BOOST (Bone marrow transfer to enhance ST-elevation infarct regeneration) trial. *Circulation*, *113*(10), 1287–1294. https://doi.org/10.1161/CIRCULATIONAHA.105.575118

Mol, E. A., Lei, Z., Roefs, M. T., Bakker, M. H., Goumans, M. J., Doevendans, P. A., Dankers, P. Y. W., Vader, P., & Sluijter, J. P. G. (2019). Injectable Supramolecular Ureidopyrimidinone Hydrogels Provide Sustained Release of Extracellular Vesicle Therapeutics. *Advanced Healthcare Materials*, *8*(20). https://doi.org/10.1002/adhm.201900847

Monteiro, N., Thrivikraman, G., Athirasala, A., Tahayeri, A., França, C. M., Ferracane, J. L., & Bertassoni, L. E. (2018). Photopolymerization of cell-laden gelatin methacryloyl hydrogels using a dental curing light for regenerative dentistry. *Dental Materials*, *34*(3), 389–399. https://doi.org/10.1016/j.dental.2017.11.020

Montgomery, M., Ahadian, S., Davenport Huyer, L., lo Rito, M., Civitarese, R. A., Vanderlaan, R. D., Wu, J., Reis, L. A., Momen, A., Akbari, S., Pahnke, A., Li, R. K., Caldarone, C. A., & Radisic, M. (2017). Flexible shape-memory scaffold for minimally invasive delivery of functional tissues. *Nature Materials*, *16*(10), 1038–1046. https://doi.org/10.1038/nmat4956

Pezzana, C., Agnely, F., Bochot, A., Siepmann, J., & Menasché, P. (2021). Extracellular Vesicles and Biomaterial Design: New Therapies for Cardiac Repair. In *Trends in Molecular Medicine* (Vol. 27, Issue 3, pp. 231–247). Elsevier Ltd. https://doi.org/10.1016/j.molmed.2020.10.006

Piluso, S., Flores Gomez, D., Dokter, I., Moreira Texeira, L., Li, Y., Leijten, J., van Weeren, R., Vermonden, T., Karperien, M., & Malda, J. (2020). Rapid and cytocompatible cell-laden silk hydrogel formation: Via riboflavin-mediated crosslinking. *Journal of Materials Chemistry B*, *8*(41), 9566–9575. https://doi.org/10.1039/d0tb01731k

Pudkon, W., Laomeephol, C., Damrongsakkul, S., Kanokpanont, S., & Ratanavaraporn, J. (2021). Comparative study of silk fibroin-based hydrogels and their potential as material for 3-dimensional (3d) printing. *Molecules*, *26*(13). https://doi.org/10.3390/molecules26133887

Rahali, K., ben Messaoud, G., Kahn, C. J. F., Sanchez-Gonzalez, L., Kaci, M., Cleymand, F., Fleutot, S., Linder, M., Desobry, S., & Arab-Tehrany, E. (2017). Synthesis and characterization of nanofunctionalized gelatin methacrylate hydrogels. *International Journal of Molecular Sciences*, *18*(12). https://doi.org/10.3390/ijms18122675

Rezaie, J., Rahbarghazi, R., Pezeshki, M., Mazhar, M., Yekani, F., Khaksar, M., Shokrollahi, E., Amini, H., Hashemzadeh, S., Sokullu, S. E., & Tokac, M. (2019). Cardioprotective role of extracellular vesicles: A highlight on exosome beneficial effects in cardiovascular diseases. In *Journal of Cellular Physiology* (Vol. 234, Issue 12, pp. 21732–21745). Wiley-Liss Inc. https://doi.org/10.1002/jcp.28894

Ritchie, H., & Roser, M. (2018). *Causes of death*. https://ourworldindata.org/causes-of-death

Rodriguez, M. J., Brown, J., Giordano, J., Lin, S. J., Omenetto, F. G., & Kaplan, D. L. (2017). Silk based bioinks for soft tissue reconstruction using 3-dimensional (3D) printing with in vitro and in vivo assessments. *Biomaterials*, *117*, 105–115. https://doi.org/10.1016/j.biomaterials.2016.11.046

Rogers, R. G., Ciullo, A., Marbán, E., & Ibrahim, A. G. (2020). Extracellular Vesicles as Therapeutic Agents for Cardiac Fibrosis. In *Frontiers in Physiology* (Vol. 11). Frontiers Media S.A. https://doi.org/10.3389/fphys.2020.00479

Sakai, S., Yoshii, A., Sakurai, S., Horii, K., & Nagasuna, O. (2020). Silk fibroin nanofibers: a promising ink additive for extrusion three-dimensional bioprinting. *Materials Today Bio*, *8*. https://doi.org/10.1016/j.mtbio.2020.100078

Singh, Y. P., Bandyopadhyay, A., & Mandal, B. B. (2019). 3D Bioprinting Using Cross-Linker-Free Silk-Gelatin Bioink for Cartilage Tissue Engineering. *ACS Applied Materials and Interfaces*, *11*(37), 33684–33696. https://doi.org/10.1021/acsami.9b11644

Sluijter, J. P. G., Davidson, S. M., Boulanger, C. M., Buzás, E. I., de Kleijn, D. P. V., Engel, F. B., Giricz, Z., Hausenloy, D. J., Kishore, R., Lecour, S., Leor, J., Madonna, R., Perrino, C., Prunier, F., Sahoo, S., Schiffelers, R. M., Schulz, R., van Laake, L. W., Ytrehus, K., & Ferdinandy, P. (2018). Extracellular vesicles in diagnostics and therapy of the ischaemic heart: Position Paper from the Working Group on Cellular Biology of the Heart of the European Society of Cardiology. In *Cardiovascular Research* (Vol. 114, Issue 1, pp. 19–34). Oxford University Press. https://doi.org/10.1093/cvr/cvx211

Smyth, T., Kullberg, M., Malik, N., Smith-Jones, P., Graner, M. W., & Anchordoquy, T. J. (2015). Biodistribution and delivery efficiency of unmodified tumor-derived exosomes. *Journal of Controlled Release*, *199*, 145–155. https://doi.org/10.1016/j.jconrel.2014.12.013

Spicer, C. D. (2020). Hydrogel scaffolds for tissue engineering: The importance of polymer choice. In *Polymer Chemistry* (Vol. 11, Issue 2, pp. 184–219). Royal Society of Chemistry. https://doi.org/10.1039/c9py01021a

Spicer, C. D., Pashuck, E. T., & Stevens, M. M. (2018). Achieving Controlled Biomolecule-Biomaterial Conjugation. In *Chemical Reviews* (Vol. 118, Issue 16, pp. 7702–7743). American Chemical Society. https://doi.org/10.1021/acs.chemrev.8b00253

Stojkov, G., Niyazov, Z., Picchioni, F., & Bose, R. K. (2021). Relationship between Structure and Rheology of Hydrogels for Various Applications. *Gels*, *7*(4), 255. https://doi.org/10.3390/gels7040255

Sukul, M., Cama, G., Dubruel, P., Janne, &, Reseland, E., & Haugen, H. J. (2020). Methacrylation increase growth and differentiation of primary human osteoblasts for gelatin hydrogels. *Emergent Materials*, *3*, 559–566. https://doi.org/10.1007/s42247-020-00101-5/Published

Takahashi, Y., Nishikawa, M., Shinotsuka, H., Matsui, Y., Ohara, S., Imai, T., & Takakura, Y. (2013). Visualization and in vivo tracking of the exosomes of murine melanoma B16-BL6 cells in mice after intravenous injection. *Journal of Biotechnology*, *165*(2), 77–84. https://doi.org/10.1016/j.jbiotec.2013.03.013

Tomasina, C., Bodet, T., Mota, C., Moroni, L., & Camarero-Espinosa, S. (2019). Bioprinting vasculature: Materials, cells and emergent techniques. In *Materials* (Vol. 12, Issue 7). MDPI AG. https://doi.org/10.3390/ma12172701

Tondera, C., Hauser, S., Krüger-Genge, A., Jung, F., Neffe, A. T., Lendlein, A., Klopfleisch, R., Steinbach, J., Neuber, C., & Pietzsch, J. (2016). Gelatin-based hydrogel degradation and tissue interaction in vivo: Insights from multimodal preclinical imaging in immunocompetent nude mice. *Theranostics*, *6*(12), 2114–2128. https://doi.org/10.7150/thno.16614

Vettori, L., Sharma, P., Rnjak-Kovacina, J., & Gentile, C. (2020). 3D Bioprinting of Cardiovascular Tissues for In Vivo and In Vitro Applications Using Hybrid Hydrogels Containing Silk Fibroin: State of the Art and Challenges. *Current Tissue Microenvironment Reports*, *1*, 261–276. https://doi.org/10.1007/s43152-020-00026-5/Published

Wang, X., Partlow, B., Liu, J., Zheng, Z., Su, B., Wang, Y., & Kaplana, D. L. (2015). Injectable silk-polyethylene glycol hydrogels. *Acta Biomaterialia*, *12*(1), 51–61. https://doi.org/10.1016/j.actbio.2014.10.027

Wu, Y., Xiang, Y., Fang, J., Li, X., Lin, Z., Dai, G., Yin, J., Wei, P., & Zhang, D. (2019). The influence of the stiffness of GelMA substrate on the outgrowth of PC12 cells. *Bioscience Reports*, *39*(1). https://doi.org/10.1042/BSR20181748

Xiao, W., Li, J., Qu, X., Wang, L., Tan, Y., Li, K., Li, H., Yue, X., Li, B., & Liao, X. (2019). Cell-laden interpenetrating network hydrogels formed from methacrylated gelatin and silk fibroin via a combination of sonication and photocrosslinking approaches. *Materials Science and Engineering: C*, *99*, 57–67. https://doi.org/10.1016/j.msec.2019.01.079

Yang, K. H., Lindberg, G., Soliman, B., Lim, K., Woodfield, T., & Narayan, R. J. (2021). Effect of photoinitiator on precursory stability and curing depth of thiol-ene clickable gelatin. *Polymers*, *13*(11). https://doi.org/10.3390/polym13111877

Zhang, K., Zhao, X., Chen, X., Wei, Y., Du, W., Wang, Y., Liu, L., Zhao, W., Han, Z., Kong, D., Zhao, Q., Guo, Z., Han, Z., Liu, N., Ma, F., & Li, Z. (2018). Enhanced Therapeutic Effects of Mesenchymal Stem Cell-Derived Exosomes with an Injectable Hydrogel for Hindlimb Ischemia Treatment. *ACS Applied Materials and Interfaces*, *10*(36), 30081–30091. https://doi.org/10.1021/acsami.8b08449

Zhou, Y., Liu, S., Zhao, M., Wang, C., Li, L., Yuan, Y., Li, L., Liao, G., Bresette, W., Zhang, J., Chen, Y., Cheng, J., Lu, Y., & Liu, J. (2019). Injectable extracellular vesicle-released self-assembling peptide nanofiber hydrogel as an enhanced cell-free therapy for tissue regeneration. *Journal of Controlled Release*, *316*, 93–104. https://doi.org/10.1016/j.jconrel.2019.11.003

## 7. Supplementary material:

| *Day* | *Significant groups (greater %-degradation denoted in bold)* | *Significance* |
|---|---|---|
| *1* | **SF_9%** vs SilkMA_8% | * |
| *2* | n/a | |
| *4* | SF_3% vs **SilkMA_12%** | * |
| | SilkMA_4% vs **SilkMA_12%** | * |
| *7* | **GelMA_12%** vs SF_9% | * |
| | **GelMA_12%** vs SilkMA_4% | * |
| | **GelMA_12%** vs SilkMA_8% | ** |
| | **GelMA_12%** vs SilkMA_12% | ** |
| | SF_9% vs **SilkMA_4%** | * |
| | **SilkMA_4%** vs SilkMA_8% | * |
| | **SilkMA_4%** vs SilkMA_12% | * |
| *14* | n/a | |
| *21* | **GelMA_3%** vs GelMA_12% | ** |
| | **GelMA_3%** vs SF_3% | ** |
| | **GelMA_3%** vs SF_6% | ** |
| | **GelMA_3%** vs SF_9% | ** |
| | **GelMA_3%** vs SilkMA_4% | * |
| | **GelMA_3%** vs SilkMA_8% | ** |
| | **GelMA_3%** vs GelMA_12% | * |
| | **SilkMA_4%** vs SilkMA_8% | * |
| | **SilkMA_4%** vs SilkMA_12% | ** |
| *28* | **GelMA_3%** vs GelMA_6% | * |
| | **GelMA_3%** vs GelMA_12% | * |
| | **GelMA_3%** vs SF_3% | ** |
| | **GelMA_3%** vs SF_6% | ** |
| | **GelMA_3%** vs SF_9% | * |
| | **GelMA_3%** vs SilkMA_4% | ** |
| | **GelMA_3%** vs SilkMA_8% | * |
| | **GelMA_3%** vs SilkMA_12% | ** |
| | **GelMA_12%** vs SilkMA_8% | * |
| | **GelMA_12%** vs SilkMA_12% | ** |

***Supplementary table 1.*** *This table shows significant results from an ordinary two-way ANOVA comparing %-degradation between gel-types per day. Non-significant comparisons were left out. For each comparison, significance is given with asterisks, and the group featuring greater degradation is made bold to make overview easier.*

| *Time* | ***Significant groups (higher EV concentration denoted in bold)*** | ***Significance*** |
|---|---|---|
| *4 hours* | n/a | |
| *1 day* | Mesh_6% vs. **Nomesh_12%** | * |
| | Nomesh_6% vs. **Nomesh_12%** | * |
| *2 days* | Mesh_6% vs. **Nomesh_12%** | * |
| | Nomesh_6% vs. **Nomesh_12%** | * |
| *4 days* | **Mesh_3%** vs. Mesh_6% | * |
| | Mesh_6% vs. **Nomesh_12%** | * |
| | Nomesh_6% vs. **Nomesh_12%** | * |
| *7 days* | **Mesh_3%** vs. Mesh_6% | ** |
| | **Mesh_3%** vs. Nomesh_6% | * |
| | **Mesh_3%** vs. Nomesh_12% | * |
| | Mesh_6% vs. **Nomesh_12%** | * |
| | Nomesh_6% vs. **Nomesh_12%** | * |
| *14 days* | **Mesh_3%** vs. Mesh_6% | ** |
| | **Mesh_3%** vs. Nomesh_12% | * |

***Supplementary table 2. A.*** *This table shows significant results from an ordinary two-way ANOVA done on cumulative data from GelMA EV release tests assessed via fluorimetry. Groups compared were obtained from gels either with or without mesh (nomesh). Significance is denoted with asterisks. Groups featuring the higher of concentrations within the comparison are noted in bold.*

| *Time* | *Significant groups (higher EV concentration denoted in bold)* | *Significance* |
|---|---|---|
| *4 hours* | Mesh_3% vs. **Mesh_12%** | * |
| | **Mesh_12%** vs. Nomesh_3% | ** |
| | **Mesh_12%** vs. Nomesh_3% | * |
| | Nomesh_3% vs. **Nomesh_12%** | * |
| *1 day* | Mesh_3% vs. **Nomesh_3%** | **** |
| | **Mesh_3%** vs. Nomesh_6% | * |
| | Mesh_6% vs. **Mesh_12%** | ** |
| | Mesh_6% vs. **Nomesh_3%** | **** |
| | Mesh_12% vs **Nomesh_3%** | *** |
| | **Mesh_12%** vs Nomesh_6% | *** |
| | **Nomesh_3%** vs. Nomesh_6% | **** |
| | **Nomesh_3%** vs. Nomesh_12% | **** |
| *2 days* | **Mesh_3%** vs. Mesh_6% | *** |
| | **Mesh_3%** vs. Nomesh_3% | *** |
| | **Mesh_3%** vs. Nomesh_12% | *** |
| | Mesh_6% vs **Nomesh_3%** | *** |
| | **Nomesh_3%** vs. Nomesh_6% | *** |
| | **Nomesh_3%** vs Nomesh_12% | * |
| *4 days* | **Mesh_3%** vs. Mesh_6% | ** |
| | **Mesh_3%** vs. Nomesh_3% | ** |
| | **Mesh_3%** vs. Nomesh_6% | * |
| | **Mesh_3%** vs. Nomesh_12% | * |
| *7 days* | n/a | |
| *14 days* | Mesh_3% vs. **Nomesh_6%** | **** |
| | Mesh_6% vs. **Nomesh_6%** | **** |
| | Mesh_12% vs. **Nomesh_6%** | **** |
| | Nomesh_3% vs **Nomesh_6%** | **** |
| | **Nomesh_6%** vs. Nomesh_12% | **** |

***Supplementary table 2. B.*** *This table shows significant results from an ordinary two-way ANOVA done on individual data from GelMA EV release tests assessed via fluorimetry. Groups compared were obtained from gels either with or without mesh (nomesh). Significance is denoted with asterisks. Groups featuring the higher of concentrations within the comparison are noted in bold.*

| *Time* | ***Significant groups (higher EV concentration denoted in bold)*** | ***Significance*** |
|---|---|---|
| *4 hours* | Blank_nomesh_3% vs. **Blank_nomesh_12%** | **** |
| | Blank_nomesh_3% vs**. Blank_mesh_12%** | **** |
| | Blank_nomesh_3% vs. **EV_nomesh_3%** | **** |
| | Blank_nomesh_3% vs. **EV_nomesh_6%** | * |
| | Blank_nomesh_3% vs. **EV_nomesh_12%** | * |
| | Blank_nomesh_6% vs. **Blank_nomesh_12%** | **** |
| | Blank_nomesh_6% vs. **Blank_mesh_12%** | **** |
| | Blank_nomesh_6% vs. **EV_nomesh_3%** | **** |
| | **Blank_nomesh_12%** vs. Blank_mesh_3% | *** |
| | **Blank_nomesh_12%** vs. Blank_mesh_6% | * |
| | **Blank_nomesh_12%** vs. EV_mesh_3% | *** |
| | **Blank_nomesh_12%** vs. EV_mesh_6% | *** |
| | **Blank_nomesh_12%** vs. EV_mesh_12% | *** |
| | Blank_mesh_3% vs. **Blank_mesh_12%** | **** |
| | **Blank_mesh_3%** vs. EV_nomesh_3% | *** |
| | Blank_mesh_6% vs. **Blank_mesh_12%** | *** |
| | Blank_mesh_6% vs. **EV_nomesh_3%** | * |
| | **Blank_mesh_12%** vs. EV_mesh_3% | **** |
| | **Blank_mesh_12%** vs. EV_mesh_6% | **** |
| | **Blank_mesh_12%** vs. EV_mesh_12% | **** |
| | **Blank_mesh_12%** vs. EV_nomesh_6% | * |
| | **Blank_mesh_12%** vs. EV_nomesh_12% | * |
| | EV_mesh_3% vs **EV_nomesh_3%** | *** |
| | EV_mesh_6% vs. **EV_nomesh_3%** | *** |
| | EV_mesh_12% vs. **EV_nomesh_3%** | ** |

***Supplementary table 3.A.*** *This table shows significant results from an ordinary two-way ANOVA done on cumulative data from SF EV release tests via NTA. Groups compared were obtained from gels either containing EVs or controls without EVs (noted as Blank), and either with or without mesh (nomesh). Significance is denoted with asterisks. Groups featuring the higher of concentrations within the comparison are noted in bold.*

| *Time* | *Significant groups (higher EV concentration denoted in bold)* | *Significance* |
|---|---|---|
| *1 Day* | **Blank_nomesh_9%** vs. Blank_mesh_3% | ** |
| | **Blank_nomesh_9%** vs. EV_mesh_3% | * |
| | **Blank_nomesh_9%** vs. EV_mesh_6% | *** |
| | **Blank_nomesh_9%** vs. EV_mesh_9% | *** |
| | **Blank_nomesh_9%** vs. EV_nomesh_6% | ** |
| *3 Days* | Blank_nomesh_3% vs. **Blank_nomesh_6%** | ** |
| | Blank_nomesh_3% vs. **Blank_nomesh_9%** | *** |
| | Blank_nomesh_3% vs. **Blank_mesh_3%** | **** |
| | Blank_nomesh_3% vs. **EV_nomesh_9%** | * |
| | Blank_nomesh_6% vs. **Blank_mesh_9%** | *** |
| | **Blank_nomesh_6%** vs. EV_mesh_9% | * |
| | **Blank_nomesh_6%** vs. EV_nomesh_6% | * |
| | **Blank_nomesh_9%** vs. Blank_mesh_6% | **** |
| | **Blank_nomesh_9%** vs. EV_mesh_3% | ** |
| | **Blank_nomesh_9%** vs. EV_mesh_9% | ** |
| | **Blank_nomesh_9%** vs. EV_nomesh_6% | *** |
| | **Blank_mesh_3%** vs. Blank_mesh_6% | **** |
| | **Blank_mesh_3%** vs. Blank_mesh_9% | ** |
| | **Blank_mesh_3%** vs. EV_mesh_3% | **** |
| | **Blank_mesh_3%** vs. EV_mesh_6% | ** |
| | **Blank_mesh_3%** vs. EV_mesh_9% | **** |
| | **Blank_mesh_3%** vs. EV_nomesh_3% | ** |
| | **Blank_mesh_3%** vs. EV_nomesh_6% | **** |
| | Blank_mesh_6% vs. **EV_nomesh_9%** | *** |
| | EV_nomesh_6% vs. **EV_nomesh_9%** | * |

***Supplementary table 3.B.*** *This table shows significant results from an ordinary two-way ANOVA done on cumulative data from SF EV release tests via NTA. Groups compared were obtained from gels either containing EVs or controls without EVs (noted as Blank), and either with or without mesh (nomesh). Significance is denoted with asterisks. Groups featuring the higher of concentrations within the comparison are noted in bold.*

| *Time* | *Significant groups (higher EV concentration denoted in bold)* | *Significance* |
|---|---|---|
| *7 Days* | Blank_nomesh_3% vs. **Blank_mesh_9%** | ** |
| | Blank_nomesh_6% vs. **Blank_nomesh_9%** | * |
| | Blank_nomesh_6% vs. **Blank_mesh_9%** | ** |
| | **Blank_nomesh_9%** vs. EV_mesh_6% | ** |
| | Blank_mesh_3% vs. **Blank_mesh_9%** | **** |
| | Blank_mesh_3% vs. **EV_nomesh_9%** | * |
| | **Blank_mesh_9%** vs. EV_mesh_6% | **** |
| *14 Days* | **Blank_nomesh_6%** vs. EV_nomesh_3% | * |
| | **Blank_nomesh_9%** vs. EV_nomesh_3% | * |

***Supplementary table 3.C.*** *This table shows significant results from an ordinary two-way ANOVA done on cumulative data from SF EV release tests via NTA. Groups compared were obtained from gels either containing EVs or controls without EVs (noted as Blank), and either with or without mesh (nomesh). Significance is denoted with asterisks. Groups featuring the higher of concentrations within the comparison are noted in bold.*

| **Significant groups (higher EV concentration denoted in bold)** | **Significance** |
|---|---|
| *SF_3% static_nomesh vs.* ***SF_6% dynamic_EV_nomesh*** | ** |
| ***SF_3% static_nomesh*** *vs. SF_6% dynamic_EV_mesh* | **** |
| *SF_3% static_nomesh vs.* ***SF_9% static_EV_mesh*** | * |
| *SF_3% static_mesh vs.* ***SF_6%_dynamic_EV_nomesh*** | ** |
| *SF_3% static_mesh vs.* ***SF_6%_dynamic_EV_mesh*** | **** |
| *SF_3%_dynamic_control_nomesh vs.* ***SF_6%_dynamic_EV_nomesh*** | ** |
| ***SF_3%_dynamic_control_nomesh*** *vs. SF_6%_dynamic_EV_mesh* | **** |
| *SF_3%_dynamic_control_nomesh vs.* ***SF_9% static_EV_mesh*** | * |
| *SF_3%_dynamic_control_mesh vs.* ***SF_3%_dynamic_EV_nomesh*** | * |
| *SF_3%_dynamic_control_mesh vs.* ***SF_6%_dynamic_EV_nomesh*** | *** |
| *SF_3%_dynamic_control_mesh vs.* ***SF_6%_dynamic_EV_mesh*** | **** |
| *SF_3%_dynamic_control_mesh vs.* ***SF_9%_static_EV_mesh*** | ** |
| ***SF_3%_dynamic_EV_nomesh*** *vs. SF_6%_static_EV_nomesh* | * |
| *SF_3%_dynamic_EV_nomesh vs.* ***SF_6%_dynamic_EV_mesh*** | *** |
| ***SF_3%_dynamic_EV_nomesh*** *vs. SF_9%_dynamic_control_nomesh* | * |
| *SF_3% dynamic_EV_mesh vs.* ***SF_6%_dynamic_EV_mesh*** | **** |
| *SF_6%_static_EV_nomesh vs.* ***SF_6%_dynamic_EV_nomesh*** | *** |
| *SF_6%_static_EV_nomesh vs.* ***SF_6%_dynamic_EV_mesh*** | **** |
| *SF_6%_static_EV_nomesh vs.* ***SF_9%_static_EV_mesh*** | ** |
| *SF_6%_static_EV_mesh vs.* ***SF_6%_dynamic_EV_mesh*** | **** |
| *SF_6%_dynamic_control_nomesh vs.* ***SF_6%_dynamic_EV_mesh*** | **** |
| *SF_6%_dynamic_control_mesh vs.* ***SF_6%_dynamic_EV_nomesh*** | ** |
| *SF_6%_dynamic_control_mesh vs.* ***SF_6%_dynamic_EV_mesh*** | **** |
| *SF_6%_dynamic_control_mesh vs.* ***SF_9%_static_EV_mesh*** | * |
| ***SF_6%_dynamic_EV_nomesh*** *vs. SF_9%_static_EV_nomesh* | * |
| ***SF_6%_dynamic_EV_nomesh*** *vs. SF_9%_dynamic_control_nomesh* | ** |
| ***SF_6%_dynamic_EV_nomesh*** *vs. SF_9%_dynamic_control_mesh* | *** |
| ***SF_6%_dynamic_EV_nomesh*** *vs. SF_9%_dynamic_EV_nomesh* | ** |
| ***SF_6%_dynamic_EV_nomesh*** *vs. SF_9%_dynamic_EV_mesh* | * |
| ***SF_6%_dynamic_EV_mesh*** *vs. SF_9%_static_EV_nomesh* | **** |
| ***SF_6%_dynamic_EV_mesh*** *vs. SF_9%_static_EV_mesh* | ** |
| ***SF_6%_dynamic_EV_mesh*** *vs. SF_9%_dynamic_control_nomesh* | **** |
| ***SF_6%_dynamic_EV_mesh*** *vs. SF_9%_dynamic_control_mesh* | **** |
| ***SF_6%_dynamic_EV_mesh*** *vs. SF_9%_dynamic_EV_nomesh* | **** |
| ***SF_6%_dynamic_EV_mesh*** *vs. SF_9%_dynamic_EV_mesh* | **** |
| ***SF_9%_static_EV_mesh*** *vs. SF_9%_dynamic_control_mesh* | ** |

***Supplementary table 4.*** *This table shows significant results from an ordinary two-way ANOVA done on dynamic EV-release data obtained via NTA. Groups compared were obtained from gels either containing EVs or controls without EVs (noted as control), and either with or without mesh (mesh/nomesh). Significance is denoted with asterisks. Groups featuring the higher of concentrations within the comparison are noted in bold.*

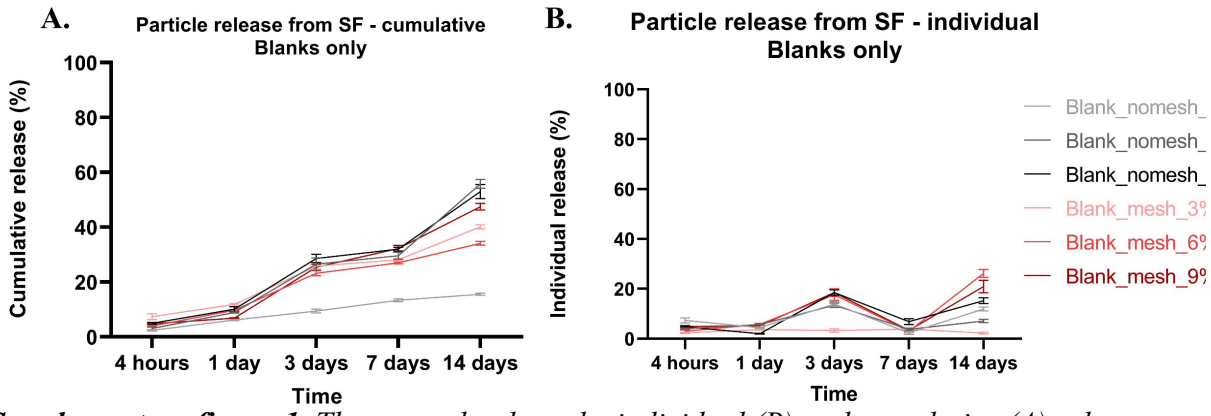


***Supplementary figure 1.*** *These graphs show the individual (B) and cumulative (A) release patterns of particles from the SF EV release tests done with nanoparticle tracking analysis. The groups represented are control groups without EVs. Please note that the degree of particle release (%) has been calculated as though samples had the same load of EVs as test samples in order to draw comparisons between samples with and without EVs.*

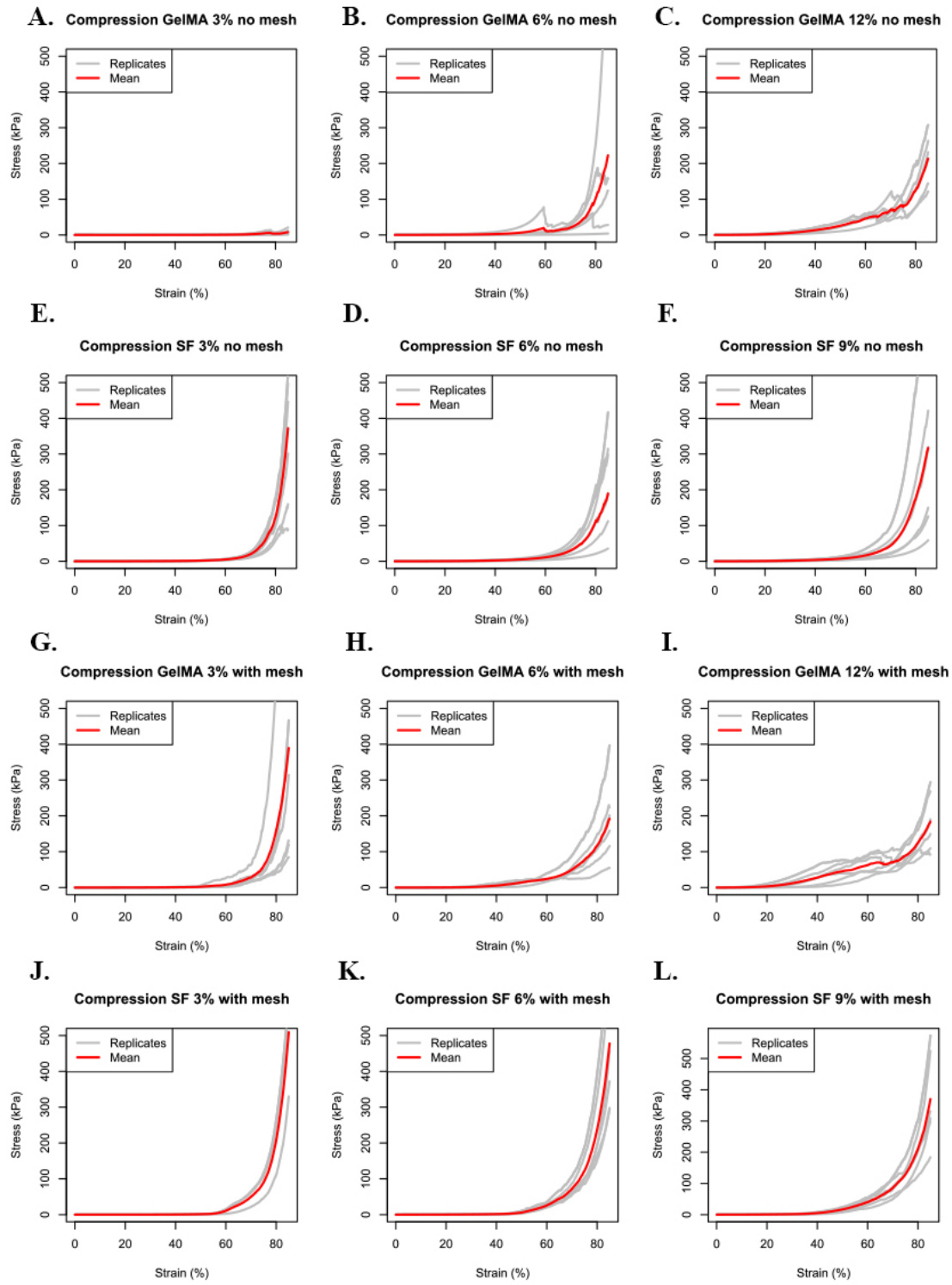


***Supplementary figure 2.*** *Shows individual and mean results from compression tests for each gel type. Grey lines denote each replicate, while red lines represent the mean of replicates for that gel type. Note that a rolling average of 25 has been applied over each sample's measurements.*

| *Gel-type* | *Young's modulus (kPa)* | *Yield strength (kPa)* |
|---|---|---|
| *GelMA 3% no mesh* | 4.9882 ± 3.9731 | 0.1653 ± 0.2517 |
| *GelMA 6% no mesh* | 102.2125 ± 109.886 | 1.4357 ± 1.5661 |
| *GelMA 12% no mesh* | 151.7501 ± 39.7993 | 16.9933± 32.9258 |
| *SF 3 % no mesh* | 121.622 ± 55.3376 | 0.3479 ± 0.0906 |
| *SF 6 % no mesh* | 119.1404 ± 67.9628 | 0.5591 ± 0.4643 |
| *SF 9% no mesh* | 171.0325 ± 153.7611 | 1.4783 ± 2.7390 |
| *GelMA 3% with mesh* | 157.452 ± 183.9022 | 0.2699 ± 0.2417 |
| *GelMA 6% with mesh* | 130.2543 ± 66.3869 | 0.2879 ± 0.3161 |
| *GelMA 12% with mesh* | 157.6814 ± 48.2938 | 15.7380 ± 37.4156 |
| *SF 3% with mesh* | 374.9167 ± 323.1705 | 0.1562 ± 0.1140 |
| *SF 6% with mesh* | 246.5074 ± 95.2028 | 0.4772± 0.3491 |
| *SF 9% with mesh* | 232.5998 ± 74.6307 | 0.5296 ± 0.3214 |

***Supplementary table 5.*** *Mean and standard deviation of Young's moduli and yield strengths computed from results of compression tests per gel type with and without mesh.*

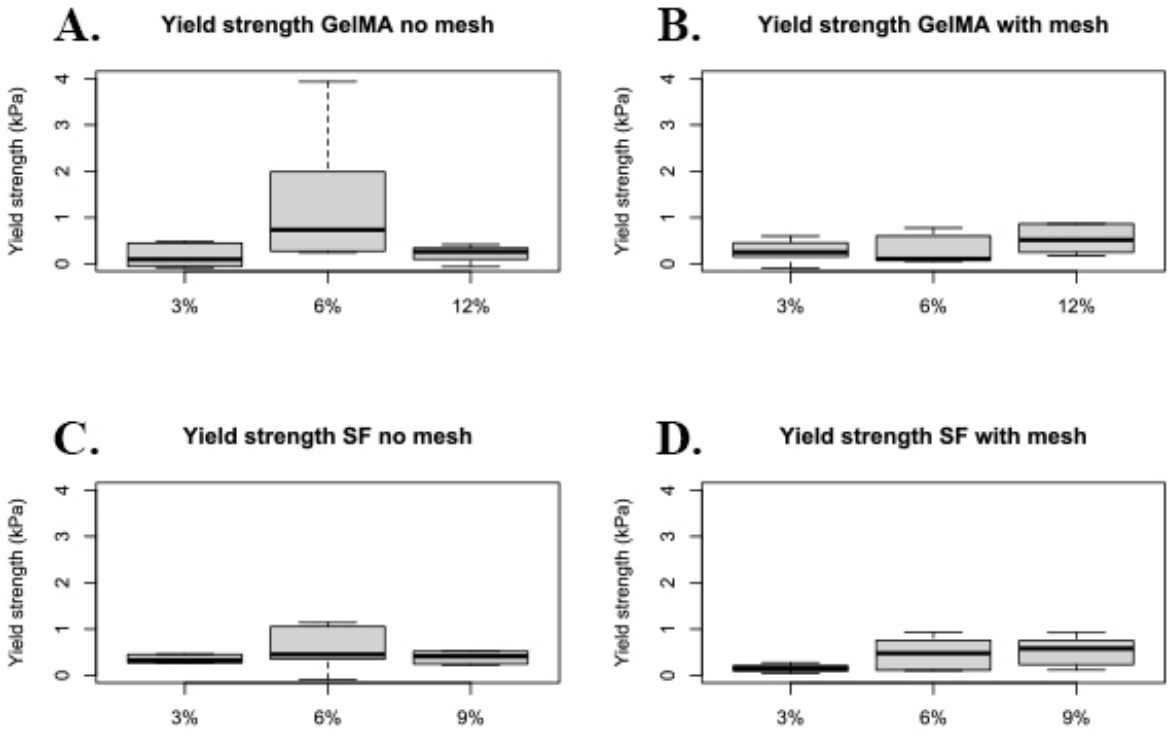


***Supplementary figure 3.*** *Box plots showing five-number summaries of yield strengths for each gel type with and without meshes, calculated from results of compression tests.*

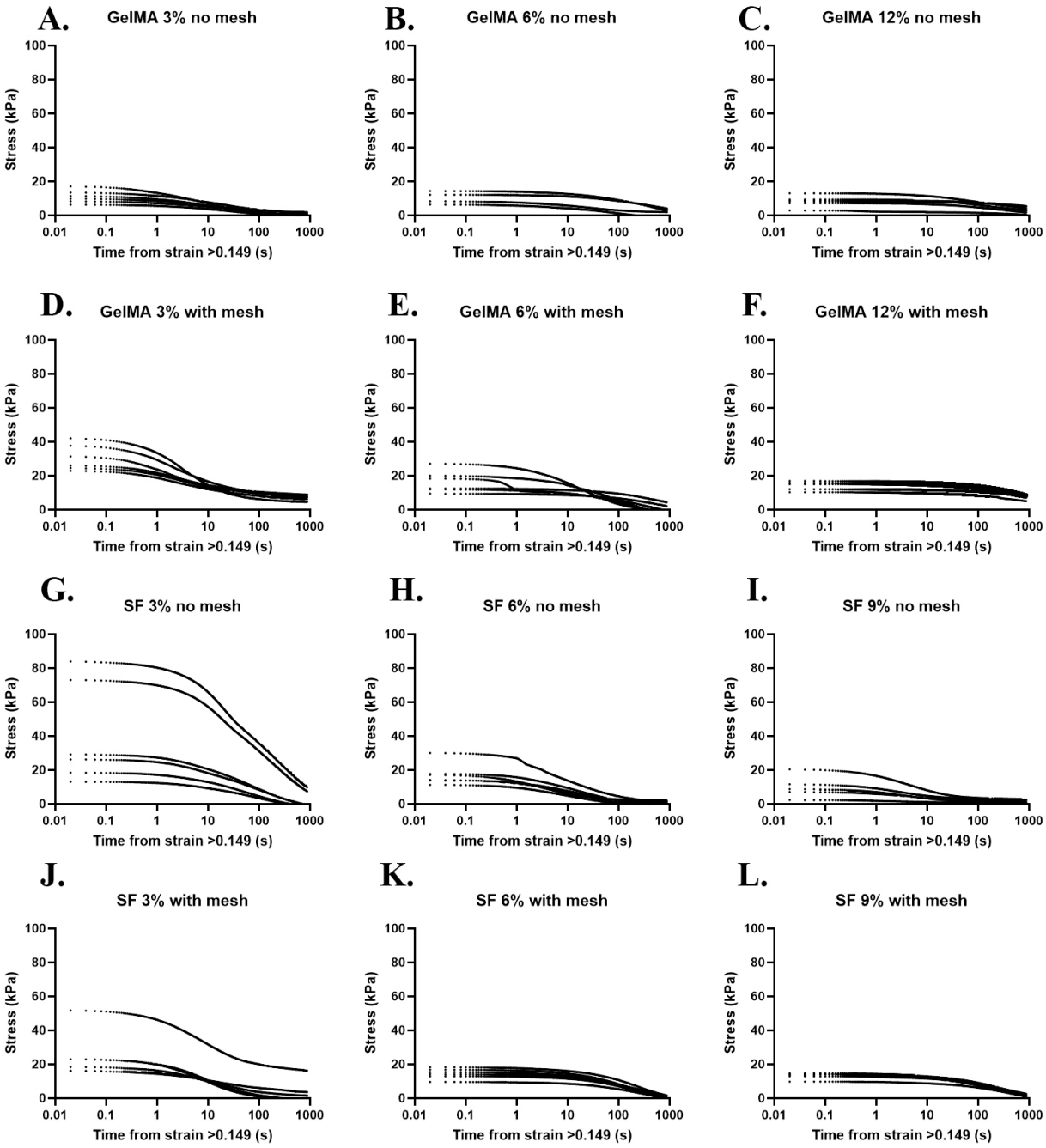


***Supplementary figure 4.*** *Stress-time curves showing results of stress-relaxation tests showing each replicate per gel-type with and without meshes. Note that a rolling average of 25 has been applied over each replicate's measurements.*

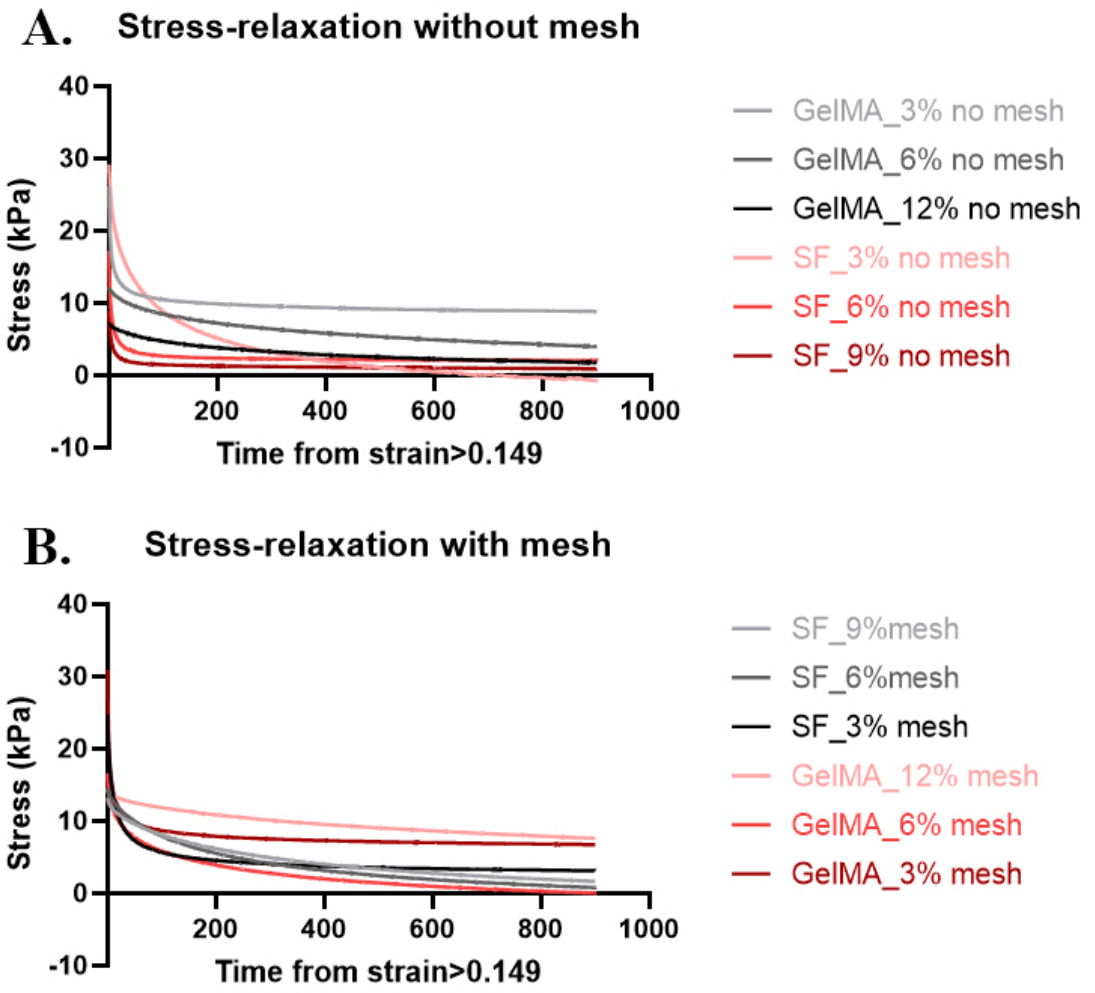


***Supplementary figure 5.*** *Graphs showing a representative stress-relaxation curve from an individual sample (so not averaged) on a non-logarithmic scale.* ***A.*** *Shows stress-relaxation curves for samples without meshes.* ***B.*** *Shows stress-relaxation curves for samples with meshes. It is difficult to compare relaxation periods using a non-logarithmic scale, as most relaxation occurs within the first minute or so.*

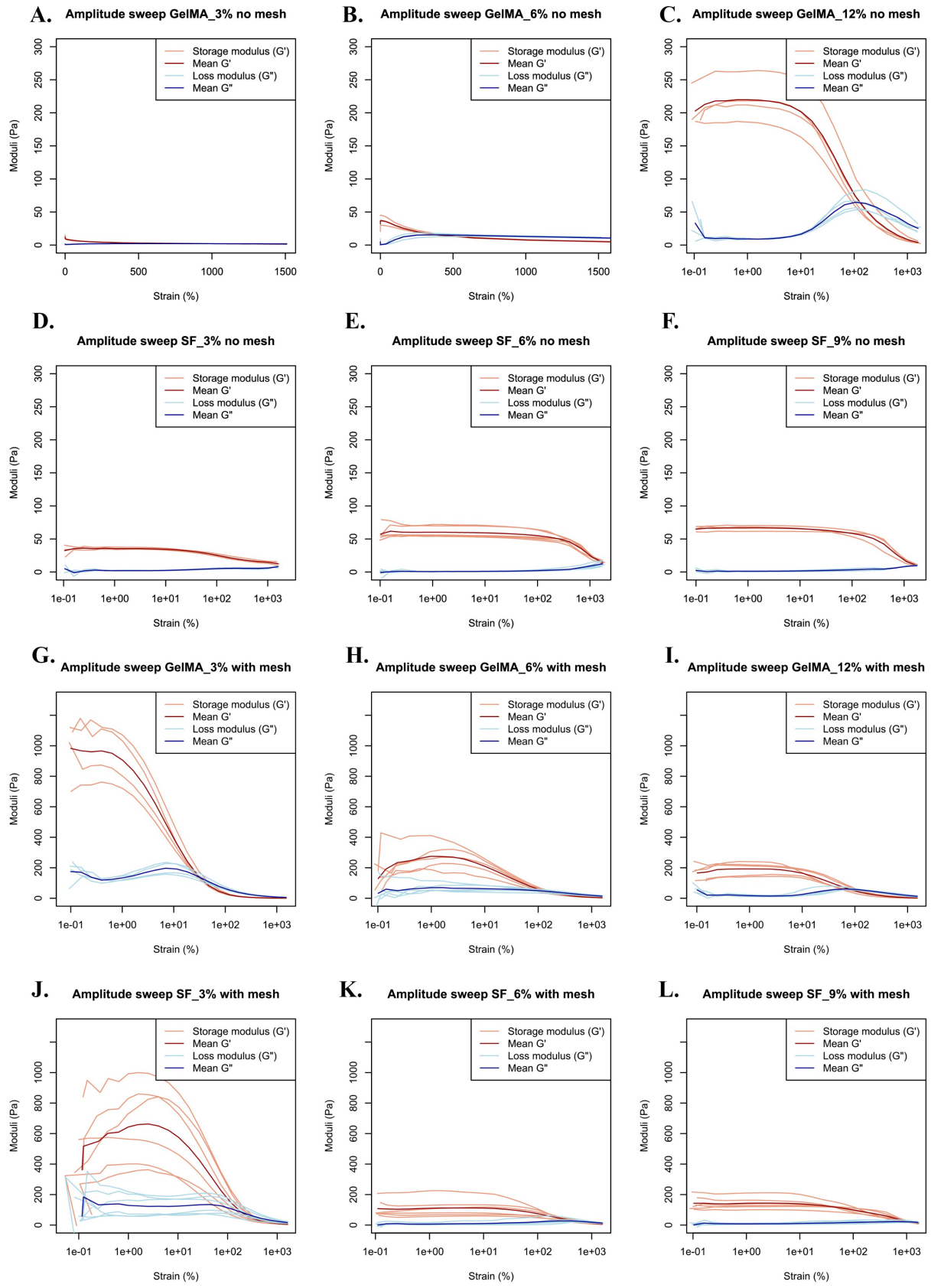


***Supplementary figure 6.*** *Shows the values for storage and loss moduli dependent on strain, gel-type, gel concentration, and mesh presence during the amplitude sweeps. Lighter colours indicate replicate values, while darker colours indicate means. Please note that the scale of the y-axis differs between gels with and without meshes, this avoid illegibility of the graphs.*

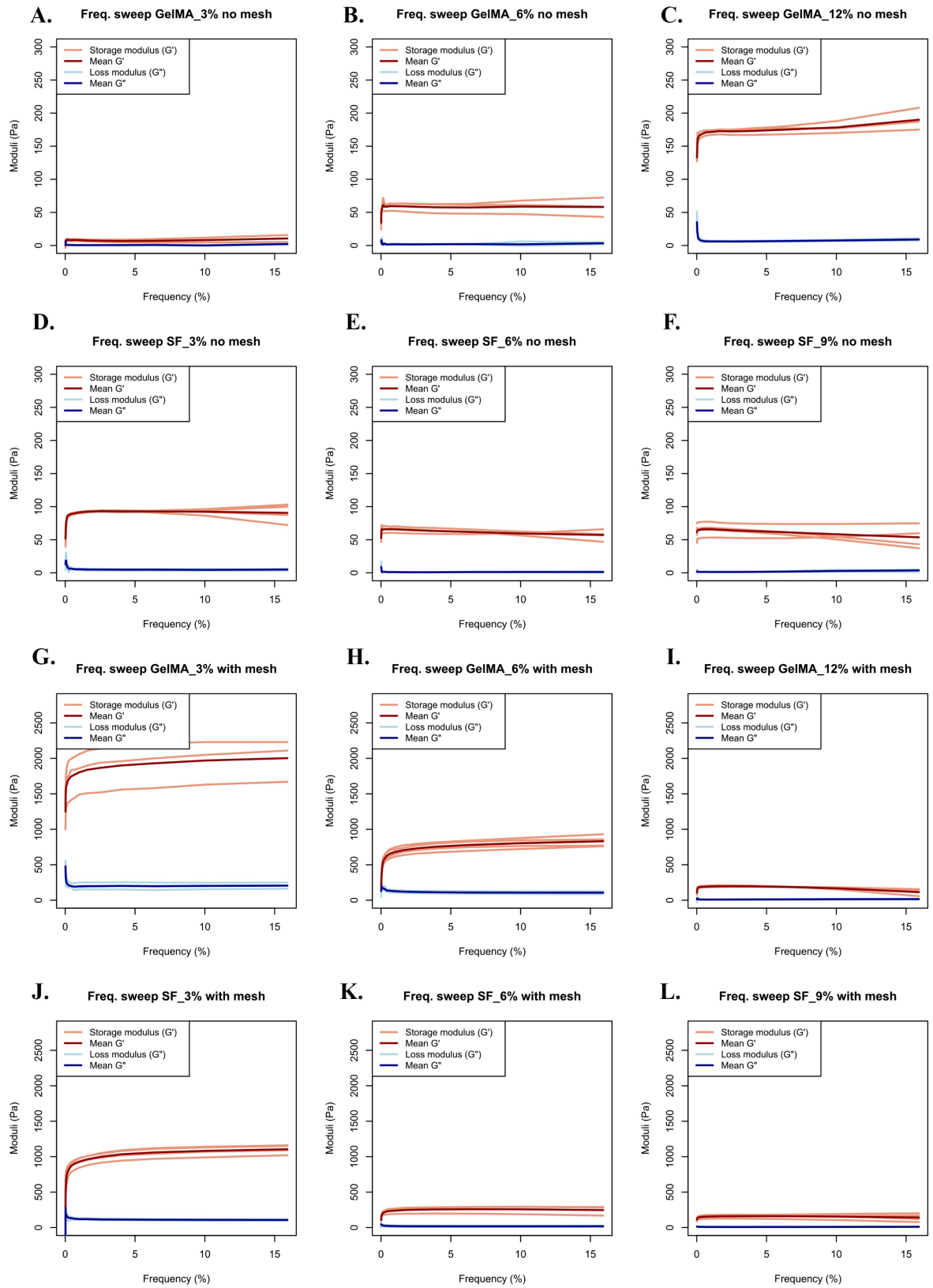


***Supplementary figure 7.*** *Curves showing frequency dependence for loss and storage moduli per gel type with and without meshes, kept under a constant 1% strain. Lighter colours indicate replicate values, while darker colours indicate means. Please note that y-axis differ in scale for samples with and without meshes in order to maintain legibility.*